SPATIALLY CONTROLLED FE ISOTOPE VARIATIONS AT TORRES DEL PAINE

BY

NORBERT ARTUR GAJOS

THESIS

Submitted in partial fulfillment of the requirements
for the degree of Master of Science in Geology
in the Graduate College of the
University of Illinois at Urbana-Champaign, 2014

Urbana, Illinois

Adviser:

Professor Craig Lundstrom

Abstract

Recent advances in mass-spectrometry have led to identification of systematic trends of changing non-traditional stable isotope ratios in igneous rocks with differentiation index. We present new Fe isotope data for the Torres del Paine igneous complex in southern Chile. The multi-composition pluton consists of a 1.5 km vertical exposure of homogenous granite overlying a contemporaneous and possibly cogenetic 0.5 km mafic gabbro suite. This first-of-its-kind spatially dependent Fe isotope investigation of a convergent margin related pluton aims to understand the nature of granite and silicic igneous rock formation.

Samples were collected along four well defined spatial transects, focusing on major plutonic contacts between the country rock, granite and mafic units. Results collected by bracketed double spike MC-ICP-MS (2σ precision of ±0.04) show a trend of increasing $\delta^{56}Fe$ with increasing silica content as well as a systematic increase in $\delta^{56}Fe$ away from the mafic base of the pluton. Importantly, the marginal Torres del Paine granites are isotopically heavier ($\delta^{56}Fe$= +0.25 ± 0.02 2se) compared to granites found in the interior pluton ($\delta^{56}Fe$= +0.17 ± 0.02 2se). Cerro Toro country rock values are isotopically light ($\delta^{56}Fe$= +0.04 ± 0.04 2σ).

The process responsible for Fe isotope variations remains debated but has been suggested to reflect four mechanisms: (1) crustal assimilation, (2) fractional crystallization, (3) late stage fluid exsolution and (4) thermal migration. Assimilation of isotopically light country rock would not produce the isotopically heavy Torres del Paine granites. Likewise, experimentally determined equilibrium fractionation factors argue against fractional crystallization producing the isotopically heavy granites. Loss of a magnetite equilibrated Fe-bearing fluid would enrich the high silica granites in isotopically heavy Fe; however, the need for unrealistically high amounts of fluid related Fe loss argues against a late stage fluid exsolution fractionation mechanism. Finally, temperature gradient driven isotope fractionation fits well with the top-down pluton emplacement sequence found by Michel et al. (2008) and Leuthold et al. (2012) and explains the spatial distribution of Fe isotope values found with depth in the pluton. We conclude that temperature gradient driven differentiation is the most likely process producing Fe isotope ratio variations in the Torres del Paine pluton. Findings from Torres del Paine have large implications for pluton emplacement, magma differentiation and the formation of granite in particular and continental crust in general.

Acknowledgements

I owe the success of the Torres del Paine project to many individuals. Foremost, I would like to thank my advisor Dr. Craig Lundstrom for five years of continuous guidance and the opportunity to study and sample the Torres del Paine pluton in Patagonia. I would also like to thank my committee members Dr. Tom Johnson and Dr. Michael Stewart for constant positive reinforcement and helpful feedback, as well as Dr. Peter Michael from the University of Tulsa for giving us access to his tremendous Torres del Paine rock powder collection.

I thank the people at CONAF (Chilean National Forest Corporation) for giving us free range over Torres del Paine National Park and allowing us to sample their most precious natural wonder. I would like to thank Nick Huggett, Valentina Hanna and Florencia Rosas Sotomayor for being brave and unyielding field assistants in the face of extreme weather and terrain. The samples they helped collect were indispensable to the success of the project. For sample preparation and sample characterization help, I thank my industrious undergraduate assistant Kyle Rehak. Additionally, I would like to thank the entire graduate geochemistry group Gideon Bartov, Kelsey Kehoe, Noah Jemison, Nick Huggett, Theodore Grimm, Anirban Basu, Katelyn Zatwarnicki, Xiangli Wang and Alyssa Shiel for their companionship and constant help while working in the lab and on the Multi-Collector. I thank my family and friends for continuous support during my time at the University of Illinois.

Finally, I would like to thank the entire Geology Department faculty and administrative staff, specifically, Marilyn Whalen, Lana Holben, Lori Baker and Shelly Campbell for making my six years at the University of Illinois some of the most memorable years of my life. Generous funding for this project came from the University of Illinois Geology department and the Roscoe Jackson field work endowment.

Table of Contents

Introduction

The composition of the upper crust is equivalent to the average composition of convergent margin granodiorite plutons (Rudnick and Gao, 2003). This correspondence suggests that water-rich subduction zone magmatism in general and plutonism in particular creates buoyant continental crust (Taylor 1965). Despite major developments in our understanding of subduction zone dynamics and mineral-melt interaction, the mechanisms responsible for pluton emplacement and magmatic differentiation are still disputed. Because the continental crust is integrally connected to plate tectonics and the evolution of life onto land, understanding the origin of convergent margin plutons and magmatic differentiation remains a fundamental question in geology.

Controversy over the origin of granitoids in the early 20th century revolved around whether granites were igneous rocks formed by crystallization from a magma, or whether they were metamorphic rocks formed by metasomatic conversion of precursor rocks. Experiments performed by Tuttle and Bowen (1958) on the $NaAlSi_3O_8$-$KAlSi_3O_8$-SiO_2-H_2O system show that granites and rhyolites from around the world plot coincident with the experimentally determined minimum melt composition coexisting with quartz and feldspar (Figure 1). These experiments led to the general acceptance that granites have an igneous origin that is controlled by thermodynamic equilibrium and not by metasomatic processes. The mechanism subsequently used to interpret the igneous origin of granites was partial melting and fractional crystallization. Yet fractional crystallization and partial melting fail to explain the relationship between granites and these experiments. In order to produce granite by these two mechanisms the minimum melt must be mechanically separated from an existing quartz-feldspar assemblage. In other words, making granite by either of these processes requires a crystal pile already containing quartz and feldspar. If mantle derived subduction zone melts are mafic or intermediate in origin, the question "how do felsic igneous rocks form?" is thus fundamentally overlooked by relying on a mechanism that involves melting from a preexisting felsic composition.

High resolution dating of convergent margin related plutons likewise has reopened questions about the timescales and mechanisms of pluton emplacement. Conventionally plutons are thought of as massive bodies of melt that are rapidly injected into the shallow crust (Buddington, 1959; Petford et al., 2000). However, geochronologic data argue against granitoids forming by crystallizing from big km size pulses of magma (Glazner et al., 2004). Over the last decade, high precision U-Pb

zircon dating methods have revealed resolvable age variations within individual plutons (Coleman et al., 2004). Work on the Toulumne Intrusive Suite (Coleman et al., 2004), Rio Honda complex (Tappa et al., 2011), Torres del Paine pluton (Michel et al., 2008; Leuthold et al., 2012) and Manaslu pluton (Harrison et al., 1999) document consistently younger dates toward either the interior of the pluton, or with increasing depth within the pluton. These variations in age suggest that plutons assemble incrementally in an accumulation of sills and dikes over an extended period of time (Annen et al. 2006). Unlike diapiric models, incremental injection models are consistent with crustal deformation rates, cooling rates and the timescales observed in plutons (Glazner, 2004). Yet, incremental models still struggle to explain how emplacement and magmatic differentiation are related; it is well established that plutons often maintain systematic compositional zoning over km scales that are difficult to reconcile with incremental assembly.

In an attempt to merge incremental pluton assembly and compositional differentiation into one process, Lundstrom (2009) proposed an alternative convergent margin pluton formation model, named Thermal Migration Zone Refining (TMZR). TMZR combines a top-down incremental pluton emplacement process with thermal migration in order to produce a zoned convergent margin pluton. Thermal migration refers to compositional differentiation by diffusive transport driven by mineral-melt equilibrium controls at different temperatures (Lesher and Walker, 1988; Walker et al., 1988). Laboratory experiments of this process show that andesite containing 4 wt.% water in a temperature gradient can self-differentiate with granite forming at the cold end of the gradient (Huang et al., 2009). Importantly, the thermal migration process appears to closely resemble observed compositional trends of igneous differentiation in zoned convergent margin plutons (Huang et al., 2009).

The discovery of systematic variations in Fe isotopes with increasing index of magmatic differentiation (SiO_2 content) provide us with a new tool for investigating plutonic processes. Recent Fe isotope studies show a consistent relationship between isotopic fractionation and indices of magmatic differentiation where, high silica granites and rhyolites are isotopically heavier than silica intermediate and mafic rocks (Figure 2) (Poitrasson and Freydier, 2005; Poitrasson, 2006; Heimann et al., 2008; Schoenberg and von Blanckenberg, 2007; Schuessler et al., 2009). The factors responsible for Fe isotope variations in igneous rocks remain debated but have been attributed to four mechanisms: (1) crustal assimilation, (2) fractional crystallization (Schoenberg and von Blanckenberg, 2007; Schuessler et al., 2009; Savage et al., 2011 and 2012), (3) late stage fluid

exsolution (Poitrasson and Freydier, 2005; Heimann et al., 2008) and (4) temperature gradient driven differentiation (Lundstrom, 2009).

This paper focuses on understanding the systematic Fe isotope variations observed in multi-composition igneous suites using samples obtained from the Torres del Paine intrusion, Southern Chile. Whereas previous isotopic investigations of igneous rocks have taken scattered sampling approaches, we present new measurements of δ^{56}Fe on a first-of-its-kind isotopic investigation using spatially controlled samples from this well constrained convergent margin related pluton. The samples collected at Torres del Paine provide an excellent distribution of rock types with a focus on well-defined sample transects across major compositional contacts, specifically, the sedimentary to granite contact, and the granite to mafic zone contact. We will show that Fe isotopes vary spatially at Torres del Paine and explore these data in the context of the isotope fractionation mechanisms mentioned above. Understanding the origin of these isotopic variations in magmatic systems can reveal important processes occurring during pluton emplacement and magmatic differentiation. Exploring incremental injection mechanisms and the origin of silicic rocks in light of new isotopic data could help unify the ideas of incremental pluton emplacement and magmatic differentiation.

Background

Non-traditional Stable Isotopes in Igneous Rocks

Until recently, it was expected that isotopic fractionation during magmatic processes was too small to observe because the magnitude of isotope fractionation scales as $1/T^2$ (Schauble, 2004). First order Fe isotope measurements on terrestrial igneous rocks performed by Beard et al. (2004) found little deviation from mean mafic earth isotopic values. However, subsequent Fe isotope studies found isotopically heavy signatures in high silica granitoids (Figure 2) (Poitrasson and Freydier, 2005; Heimann et al., 2008). Elevated Fe isotope values in granites led Poitrasson and Freydier (2005) and Heimann et al. (2008) to suggest that isotopic fractionation could be caused by a removal of a chlorine rich Fe-bearing fluid during the final stages of pluton formation. Alternatively, several studies have interpreted Fe isotope trends to be a product of fractional crystallization (Schoenberg and von Blanckenberg, 2007; Schuessler et al., 2009). Experimentally determined equilibrium isotopic fractionation factors (Bilenker et al., 2012; Shahar et al., 2008) and theoretical predictions (Polykov and Mineev, 2000) show that magnetite is isotopically heavier relative to both fayalite and silicic melt. Finally, the effects of crustal assimilation on heavy Fe isotope enrichment in high silica igneous rocks were deemed unfavorable for Fe (Schoenberg and von Blanckenberg, 2007).

Recent experiments show that thermal diffusion (temperature gradient driven diffusion) creates large isotopic fractionations in silicate melts within all element isotopic systems thus far examined. Thermal diffusion shows a consistent behavior of heavy isotope enrichment at the cold end of a temperature gradient and light isotope enrichment at the warm end of the gradient (Kyser et al., 1998; Richter et al., 2008, 2009; Huang et al., 2010). The isotopic effect occurs in both above liquidus Soret experiments and in experiments containing coexisting melt and crystals (e.g. thermal migration) (Lesher and Walker, 1988; Walker et al., 1988). Specifically, wet thermal migration experiments performed by Huang et al., 2009 show large non-traditional stable isotope variations of δ^{26}Mg and δ^{56}Fe and similar variations in light stable isotopes δ^{18}O, δ^{7}Li and δD (Bindeman et al., 2013). Although the origin of temperature gradient fractionation remains uncertain, diffusion and molecular dynamics modeling suggest a mass dependent process driven by classical mechanical effects, specifically differences in momentum between the light and heavy isotope (Lacks et al., 2011).

The systematic stable isotope fractionation pattern produced by thermal diffusion provides a unique fingerprint for distinguishing temperature gradient driven differentiation (TMZR) in magmatic systems. Specifically, if a TMZR process is operating at Torres del Paine, the Fe isotope profile of the zoned pluton should be spatially controlled, with the granites at the top of the intrusion being isotopically heavy and the diorites and gabbros at the mafic root being isotopically light (Lundstrom, 2009). Analyzing Fe isotope variations across the major compositional and geochronologic regions at Torres del Paine can therefore directly test whether temperature gradient driven differentiation and a TMZR process can occur in a convergent margin related pluton like Torres del Paine.

Geology of Torres del Paine

The Torres del Paine pluton is part of a chain of Miocene emplaced convergent margin related plutons located between two major magmatic provinces: the older Cretaceous-aged Southern Chile Patagonian Batholith to the west and the Cenozoic Plateau Basalts to the east (Michael, 1991; 1984). The glacially exposed pluton is virtually undeformed and unaltered with key sedimentary (Cretaceous Cerro Toro and Punta Barosa turbidite formations) roof contacts and granite/mafic zone contacts perfectly preserved. The multi-composition pluton consists of a 1.5 km vertical exposure of biotite-hornblende granite overlying a 0.5 km mixed diorite and gabbro suite (Paine Mafic Complex: PMC) (Figure 3) (Leuthold et al., 2012; Michael, 1991 and 1984). Michael (1991) and Leuthold et al., (2012) interpret the PMC to reflect injection of a separate mafic magma into an existing felsic intrusion. This distinctly differs from our view of the granite-PMC relationship.

Aplites are common in the upper exposures of the granite and also occur in cone sheets that extend subhorizontally (~5km) away from the pluton (Michael, 1991; 1984). The granite extends downward along the sides of PMC such that the mafic suite never directly contacts the sedimentary country rock. The contact between the PMC and granite is visibly "sharp" along both the sides and the top of the PMC, occurring horizontally at ~1100m elevation. In detail the rock type transition maintains a relatively sharp contrast in color index but often shows abundant mafic enclaves in the granite indicating interaction relationships. The top of the PMC is composed of a mixture of granitoids and monzodiorite sills. The PMC becomes more mafic with depth as it transitions into hornblende gabbros and olivine-hornblende gabbros at the base of the exposure (Leuthold et al., 2012).

High resolution CA-TIMS dating suggests that the pluton was emplaced top-down over the course of 162 ± 11ka (Michel et al., 2008; Leuthold et al., 2012). Zircon dating of the Torres del Paine granite reveals a 90kyr age difference within the granite (Michel et al., 2008). Specifically, one granite sample located along the upper margin of the pluton gives an older date (12.58 ± 0.02 Ma) compared to a granite sample located in the interior of the pluton (12.49 ± 0.02 Ma) (Michel et al., 2008). This age gap led Michel et al. (2008) to suggest the granite was emplaced incrementally over the course of three major pulses, with the oldest granite at the top and margins of the intrusion and the youngest granite overlying the granite/PMC contact. Geochronologic dates measured by Michel et al. (2008) and Leuthold et al. (2012) are illustrated in the cross section in Figure 3.

A vertical transect through the younger PMC reveals a ~41ka emplacement period between the lower hornblende gabbros and the layered diorites (Leuthold et al., 2012). Unlike the Torres del Paine granite, the PMC becomes older with depth. The layered diorites at the top of the mafic complex are the youngest rocks in the PMC with an age of 12.431±0.010 Ma. The underlying upper hornblende gabbro unit (12.434±0.009 Ma), diorite sill unit (12.453±0.010 Ma) and lower hornblende gabbro unit (12.472±0.009 Ma) at the base of the exposure have progressively older ages. Leuthold et al. (2012) interprets this aging with depth to a bottom-up sill emplacement process. However, a few outlier zircons aged up to 12.616±0.014 Ma occur within the PMC indicating inheritance or other complications to simple sequential magmatic injection.

Methods

The samples (0.5-1kg specimens) were crushed and homogenized into a fine powder for compositional and isotopic analysis. Major element compositions were determined on fused sample glasses (2:1 lithium tetraborate flux to sample ratio) using standards based EDS X-ray analysis on the UIUC JEOL 840A scanning electron microscope. Additional rock powders were obtained from Peter Michael from the University of Tulsa with major and trace element compositions published in Michael, (1984, 1991). Elemental data for Torres de Paine samples are listed in Table 1. A detailed list of sample descriptions and locations is located in Appendix A.

For Fe analysis, 40 samples were dissolved in closed Savillex beakers at 140°C using HF and HNO_3. These were dried down, treated with concentrated HNOs and HCl and dried down once more. Samples were brought up in 0.6mL 8N HCl and put through AG1-X8 anion exchange resin removing all ions besides Fe. Fe was eluted using $8HNO_3$. Fe isotope analysis was performed on the University of Illinois Nu Plasma HR-MC-ICP-MS in high resolution mode using a 57Fe-58Fe double spike technique involving separate Cr and Ni corrections. Analysis was performed using a 100 μl min^{-1} nebulizer. Resolution (M/ΔM) on ^{56}Fe was ~9000. Primary reference material IRMM-14 Fe standard was used for bracketing each analysis- the standard error on all IRMM-14 analyses was 0.02 2se showing little drift. Standard reference material BCR-2, AGV-2, RGM-1, NOD-P and UIFe were used as secondary standards. Offset and precision for standards is listed in Table 3. Precision is reported in 2σ and 2se. Per mil values were calculated using Equation 1:

Equation 1: $\delta^{56}Fe_{IRMM\text{-}14}$= (Ratio sample- Ratio standard)/(Ratio standard) *1000‰

Eighteen samples were prepared for Pb isotope analysis following methods in Gladu and Kamber (2008). 50 mg of sample were dissolved in closed Savillex beakers at 140°C using concentrated HF and HNO_3. The samples were dried down, attacked with concentrated HCl and HNO_3, brought up in 0.5mL of 0.5N HBr and loaded onto AG1-x8 anion exchange resin. Pb ions were eluted in 10.5N HCl. Pb analysis was performed on the University of Illinois Nu Plasma MC-ICP-MS in low resolution mode using admixed Tl. Analysis was performed using a 100 μl min^{-1} nebulizer. Primary reference material SRM981 Pb isotopic standard was run every three samples and BCR-2 was used as a secondary standard and interspersed with samples. The value and precision of these standards is listed in Table 2. Precision is reported in 2σ.

For Sr analysis, 40 samples were dissolved in closed Savillex beakers at 140°C using HF and HNO_3. These were dried down, treated with concentrated HNO_3 and HCl steps, brought up in 3N HNO_3 and put through Sr Spec anion exchange resin. Sr analysis was performed on the University of Illinois Nu Plasma MC-ICP-MS in low resolution mode. Analysis was performed using a 100 μl min^{-1} nebulizer aspirated into a DSN-100 desolvator. SRM987 was run every 3 samples as a primary reference material. E&A and an in-house modern Coral solution were interspersed with samples. The offset between the measured SRM987 and true was used to correct samples and the E&A and Coral results. The corrected $^{87/86}Sr$ values for Coral and E and A agree with known values indicating accuracy (Table 2). Precision is reported in 2σ and is generally +/- 0.00002.

Results

The samples collected at Torres del Paine provide an excellent distribution of rock types with a focus on well-defined sample transects across major geochronologic and compositional provinces. Major element data (along with data of Michael et al., 1984; 1991) trends show a continuum indicating a cogenetic relationship of the granite and PMC (Figure 4). We report bulk Fe, Sr and Pb isotope data for the entire intrusion and Fe data for four sampling transects: two country rock/ granite transects, one granite/PMC transect, and one PMC transect. Finally, we present a composite Spatial Fe isotope profile for the entire intrusion.

Sr and Pb isotopes

Sr and Pb isotope data are given in Table 2. Age corrections were only performed on aplites, as the corrected ages for the remainder of samples differ by less than 0.08%. $^{87/86}Sr$ strongly correlates with silica content (Figure 5). Granite samples have $^{87}Sr/^{86}Sr$ ranging from 0.70501 to 0.70860, while diorites and gabbros are less radiogenic, ranging from 0.70390 to 0.70527. Cerro Toro values have the highest $^{87}Sr/^{86}Sr$ values in the sample set ($^{87}Sr/^{86}Sr$= 0.71480 and $^{87}Sr/^{86}Sr$= 0.71002). These results generally agree well with those of Leuthold et al. (2012).

Pb isotope values are notably invariant throughout the intrusion (Figure 6). Granite, diorites and gabbros from Torres del Paine data have an average $^{208}Pb/^{204}Pb$= 38.68+/- 0.06, $^{207}Pb/^{204}Pb$= 15.63+/- 0.01 and $^{206}Pb/^{204}Pb$= 18.77+/- 0.06. Sediments have $^{208}Pb/^{204}Pb$= 38.66+/- 0.03, $^{207}Pb/^{204}Pb$= 15.64+/- 0.01 and $^{206}Pb/^{204}Pb$= 18.75+/- 0.04. These results generally agree well with those of Leuthold et al. (2012).

Fe isotope data

Bulk rock Fe isotope analysis values of Torres del Paine samples are consistent with previous data on igneous rocks showing an increase in $\delta^{56}Fe$ with increasing SiO_2 content particularly at high SiO_2 content (Figure 7). $\delta^{56}Fe$ values range from -0.05 ± 0.04‰ to +0.52 ± 0.04‰ with gabbros and diorites being the isotopically lightest and high silica granites and aplites being the isotopically heaviest. Fe isotope data for country rock, cone sheet aplites, basaltic dikes, composite dikes and veins are listed in Table 3. Notably, country rock values for both Cerro Toro country rock samples are isotopically light ($\delta^{56}Fe$= +0.03 and +0.05 ± 0.04‰). Aplites and cone sheet aplites have some of the heaviest Fe isotope signatures at Torres del Paine (aplite average $\delta^{56}Fe$= +0.36 ± 0.04‰).

Two composite dike sample pairs have isotopic values within error of each other; the mafic component of the dike has a δ^{56}Fe value of +0.17 ± 0.04‰, and the felsic interior has a value of +0.12 ± 0.04‰ Two sub-horizontal felsic sheets located within the PMC have isotopic values of δ^{56}Fe = +0.23 ± 0.04‰ and +0.36 ± 0.04‰.

Sample Transects:

We sampled along four 200m -800m linear transects that spanned the major compositional and geochronologic provinces of the intrusion. The spatial positioning of these four sample transects relative to the pluton is illustrated in Figure 3. Two transects sampled the marginal country rock/granite contact which targeted the oldest granites in the intrusion and the bordering country rock (Cerro Toro formation). Transect 1 sampled the Valle Silencio granite/country rock contact, and Transect 2 sampled the Valle Torres granite/country rock contact. Another horizontal transect sampled across the granite/PMC contact; this transect targeted the youngest granites in the intrusion and the underlying diorites and gabbros (Transect 3). The final transect (Transect 4) vertically sampled across the mafic sills of the PMC (layered diorites and two hornblende gabbro units).

Transect 1: Granite/Country Rock

The first transect was collected along the southern wall of Valle Silencio (Figure 8). Six granite samples were collected in a line starting at the brecciated country rock/granite contact and moving 1.7km into the interior of the pluton. Four samples from within the Torres del Paine granite show a constant δ^{56}Fe value of +0.25 ± 0.04‰. Two granite samples (SG-3 and SG-1) from granitic pods found in the country rock near the granite/country rock contact have relatively lighter Fe isotope values of δ^{56}Fe=+0.17 ± 0.04‰. These granites exhibit higher $^{87}Sr/^{86}Sr$ values compared to the other samples in the transect (Figure 8). The presence of country rock xenoliths in the granite suggest localized crustal assimilation along the contact.

Transect 2: Granite/Country Rock

The second country rock/granite transect was collected on the southern wall of the Valle Torres (Figure 9). The transect begins in the meta-sediments along the margin of the pluton and terminates 800m away from the contact in the Torres del Paine granite. Sample GT-Xtry, a metamorphosed mudstone country rock sample directly in contact with the granite, has a δ^{56}Fe value of +0.03 ± 0.04‰. The nine granites of the transect have a homogenous Fe isotope value (average

$\delta^{56}Fe$= +0.26 ± 0.04‰). One basaltic dike located in the granite, 100m away from the country rock contact has a $\delta^{56}Fe$ value of +0.18 ± 0.04‰.

Transect 3: Granite/PMC

One vertical granite to mafic sample transect was collected along the northern wall of the Valle Frances (Figure 10). This transect samples the youngest granite unit of the intrusion (Michel et al., 2008) which lies directly above the granite/PMC contact. The 100m vertical transect starts in the homogenous granite (three samples) and moves into the diorite sills of the PMC (four samples). The three granite samples show below average $\delta^{56}Fe$ granite values ($\delta^{56}Fe$= +0.15 ± 0.04‰). The underlying diorites are within mean mafic earth isotopic values (Poitrasson et al., 2004). A 2cm wide felsic vein running through diorite sills has $\delta^{56}Fe$ values of +0.19 ± 0.04‰.

Transect 4: PMC Transect

Our last sampling transect was collected across the PMC (Figure 11). Samples were collected top-down along a 300m vertical transect of Castillo, a small peak located in the southwest portion of the Valle Frances. Castillo features a series of alternating diorite and gabbro sills, specifically, the younger layered diorites at the top of the PMC and two separate hornblende gabbro units that make up the middle and the older base of the exposure. The layered diorites and the hornblende gabbros of the PMC are very homogenous and deviate little from mean mafic earth isotopic values (Poitrasson et al., 2004). Additionally, two granite porphyry pods at the base of Castillo have below average granite $\delta^{56}Fe$ values ($\delta^{56}Fe$= +0.21, +0.16 ± 0.04‰).

Composite Spatial Fe Isotope Distribution in Torres del Paine

Finally composite Fe isotope data from Torres del Paine reveals a spatial trend of increasing $\delta^{56}Fe$ away from the mafic root of the pluton (Figure 12). Granites near the margins of the intrusion (within 800 meters of the granite/sedimentary contact) are isotopically heavier than granites located within 100 meters of the Paine Mafic Complex. Specifically, 15 samples taken from the marginal granite have an average $\delta^{56}Fe$ of +0.25 ± 0.02 2se; whereas, 7 granite samples in the interior of the pluton taken within 100 meters of the PMC have an average $\delta^{56}Fe$= +0.17 ± 0.02 2se. Thus, the total isotopic difference between the marginal granites and the interior granites is 0.08 per mil. If isotopically heavy marginal aplites were included into the 'marginal granite' population of samples, the overall variation would be even greater (0.11 per mil). Outliers from this spatial trend include

two granite samples directly on the country rock/ granite contact ($\delta^{56}Fe$=+0.17 ± 0.04‰). Porphyritic granite pods found at the base of the PMC are categorized as granites located within 100 meters of the Paine Mafic Complex.

Discussion

The source of Fe isotope variations in igneous plutonic rocks has puzzled geochemists ever since their discovery (Poitrasson and Freydier, 2005). These small but resolvable isotopic variations are important because they occur in major rock forming elements and are clearly tied to the degree of magmatic differentiation in igneous rocks. Understanding these variations can therefore shed new light on granite and continental crust formation. The Torres del Paine pluton in southern Chile provides the perfect location for examining the relationship between Fe isotope variations in igneous rocks and compositional differentiation. The bimodal composition of the pluton and the excellent exposure of sedimentary, granite and mafic zone contacts allow for a detailed analysis of intra-plutonic Fe isotope fractionation processes. In this discussion we will assess the contribution of 1) crustal assimilation, 2) loss of a hydrous fluid, 3) fractional crystallization and 4) temperature gradient driven differentiation on Fe isotope variations in convergent margin plutons.

Crustal Assimilation

Previous discussions of the role of crustal assimilation in explaining δ^{56}Fe variations led to inferences that the assimilation did not produce isotopically heavy granites (Schoenberg and von Blanckenberg, 2007) because sedimentary reservoirs are typically isotopically light (Staubwasser et al., 2006; Beard et al., 2004). Yet prior to this study, no coupled pluton/country rock sample pairs were analyzed to directly test this idea. Field observations from Torres del Paine reveal localized assimilation of sedimentary rock along the granite and country rock contact (Michael, 1991; 1984). Sr and Pb isotopic values also suggest some degree of crustal assimilation as Sr increases with differentiation and Pb values from the Cerro Toro country rock overlap with Torres del Paine values (Figure 5 and 6). Therefore, it is important to test for isotopic contamination caused by the country rock.

Fe isotope data from Torres del Paine confirm that the isotopically heavy signatures observed in granites are not related to crustal assimilation. The Fe isotope signature of the intruded Cerro Toro turbidite formation is low in δ^{56}Fe (δ^{56}Fe = +0.05, +0.03 ± 0.04‰) compared to the Torres del Paine granite. Crustal assimilation of the isotopically light Cerro Toro formation or melt derived from isotopically light lower crustal sediments would, therefore, not produce the isotopically heavy δ^{56}Fe signature found in the Torres del Paine granite. Crustal assimilation conclusively does not explain the heavy Fe isotope signature of Torres del Paine granites.

Several granite samples collected from brecciated pods located in the country rock near the granite/country rock contact show distinctly lower $\delta^{56}Fe$ values compared to the average granite values of the Torres del Paine granite. Elevated $^{87}Sr/^{86}Sr$ values in the isotopically light near-contact granites may suggest localized mixing between the Cerro Toro country rock and the Torres del Paine granite (Figure 8). A simple mixing model comparing average Torres del Paine granite isotopic values ($\delta^{56}Fe$= 0.22 ±0.04‰) with average country rock isotopic values ($\delta^{56}Fe$= 0.04 ±0.04‰) shows that incorporating 10-20% isotopically light country rock can create the $\delta^{56}Fe$=0.17±0.04‰ observed in the isotopically light granites (Figure 13). The mixing model suggests that crustal contamination is a viable explanation for these low $\delta^{56}Fe$ and high $^{87}Sr/^{86}Sr$ near contact granites. However, the scale of isotopic interaction is minimal and restricted to the granite pods found within the country rock. Light Fe isotope enrichment of the granite due to crustal assimilation is, therefore, limited to 1-5 meters from the country rock contact.

Fractional Crystallization

Several studies attribute Fe isotope trends with differentiation to fractional crystallization (Schoenberg and von Blanckenberg, 2007; Schuessler et al., 2009). Previous work at Torres del Paine interpret the formation of the granite to some variation of fractional crystallization: in situ fractional crystallization by Michael (1984) and assimilation fractional crystallization by Leuthold et al. (2012). Testing the validity of isotopic fractionation caused by fractional crystallization is therefore vital to interpreting the origin of the pluton. The isotopic evolution of a melt during the incremental removal of ferromagnesian phases can be modeled as a Rayleigh distillation process. Analysis of mineral separates in granites shows that magnetite is isotopically heavy and responsible for the high $\delta^{56}Fe$ values of granites (Heimann et al., 2008). Thus, assessing Fe isotope fractionation during fractional crystallization requires knowing the equilibrium isotopic fractionation factor for magnetite-melt.

Fractionation factors can be measured experimentally or estimated from spectroscopy techniques. Experiments show that heavy isotopes of Fe preferentially partition into magnetite relative to other phases. Specifically, magnetite-fayalite equilibrium fractionation experiments indicate a $\varepsilon^{57}Fe_{Mag\text{-}Fay} = 0.30 \times 10^6/T^2$, where $\varepsilon = 1000\ln\alpha$ and $\varepsilon^{57}Fe_{Mag\text{-}Fay}$ is the fractionation factor between magnetite and fayalite (Shahar et al., 2009). Similarly, preliminary equilibrium magnetite-melt-fluid experiments confirm that magnetite is isotopically heavier than the co-existing melt and fluid (Bilenker et al., 2012) with a fractionation factor of $0.07‰ < \varepsilon^{56}Fe_{Mgt\text{-}Melt} < 0.2‰$ for a 700 to

1200°C temperature range. In other words, mechanically removing magnetite from a melt via a Rayleigh distillation process should leave the differentiated melt isotopically light (Figure 14). A visual best estimate for a Torres del Paine fractionation factor is $\varepsilon^{56}Fe_{Solid\text{-}Melt}$ = -0.10‰. Rayleigh crystallization, therefore, produces a modeled trend opposite to what is observed at Torres del Paine and in felsic plutons in general. Likewise, the crystallization of Fe-bearing silicates is unlikely to explain the observed Fe isotope trend. Isotopic analyses of pyroxene, biotite and hornblende mineral separates show $\delta^{56}Fe$ values that are negative or close to 0 (Heimann et al., 2008). Therefore, evidence from equilibrium isotope fractionation experiments largely argues against fractional crystallization creating the isotopically heavy granites at Torres del Paine and felsic plutons in general.

Late Stage Fluid Exsolution

Several workers have suggested that Fe isotope variations reflect fractionation occurring during removal of a chloride rich Fe-bearing fluid during the final stages of pluton formation (Heimann et al., 2008; Poitrasson and Freydier, 2005; Telus et. al., 2012). If such a fluid in equilibrium with magma containing magnetite were removed from a plutonic system, the remaining material (silicic melt plus crystals including magnetite) should become isotopically heavier (Heimann et al., 2008).

Preliminary equilibrium magnetite-fluid-melt experiments support the observation that magnetite incorporates isotopically heavier Fe relative to an equilibrium fluid: $\Delta_{fluid\text{-}magnetite}$~ -0.30‰ at 800°C (Bilenker et al., 2013). Indeed, Rayleigh distillation models using this fluid-magnetite fractionation factor can reproduce $\delta^{56}Fe$ vs FeO/FeOi for Torres del Paine data (Figure 15). However, the amount of isotopic fractionation fundamentally depends on the amount of Fe removed from the system by fluid segregation. In order to substantially change the isotopic signature of the pluton, weight percent levels of Fe would need to be mobilized into the exsolved fluid. Specifically, 35% of the Fe in the existing magnetite would have to be removed from the crystal mush pile to reproduce the Torres isotopic fractionation trend (Figure 15). However, Harker plots of Torres del Paine data argue against there being significant amounts of Fe lost to fluids at Torres del Paine. FeO content decreases linearly with increasing SiO_2 content (Figure 16) arguing for a magmatic differentiation process devoid of significant amounts of fluid loss. Similarly, constant increase in fluid mobile Rb with differentiation reinforces the idea that significant fluid loss did not affect the cooling pluton (Figure 16).

Furthermore, any realistic amount of Fe isotope fractionation via fluid removal would have to occur on top of Fe removal during fractional crystallization. Rayleigh models show that the Torres del Paine fractionation trend cannot be reproduced when the effects of fractional crystallization and fluid loss are summed together. A realistic scenario where 10% of Fe is removed via fluid loss and the remainder is removed via crystallization would drive the residual system toward isotopically lighter values (Figure 15). This is the opposite of what is observed in the Torres del Paine trend. Thus, a much larger magnetite-fluid fractionation factor would be necessary to leave the residual system isotopically heavy. Assuming 10% Fe is being equilibrated and removed from the system, the fractionation factor for magnetite-fluid would have to be ~-3.00‰ on top of the 0.18‰ fractional crystallization fractionation factor in order to reproduce the Torres del Paine fractionation trend. Such high fractionation factors are not observed in equilibrium isotope experiments. Therefore, late stage fluid exsolution likely does not cause the ubiquitous Fe isotope fractionation observed in Torres del Paine and felsic plutons in general.

Temperature Gradient Driven Differentiation

Non-traditional stable isotope variations in plutons have also been attributed to thermal diffusion occurring within a temperature gradient based differentiation process (Lundstrom, 2009). Temperature gradient experiments show that stable isotope ratios are fractionated across the gradient with heavy isotopes preferentially enriched toward the cold end of the temperature gradient. Although the reason for thermal diffusion fractionation remains debated (Huang et al., 2010; Dominguez et al., 2011; Lacks et al., 2012), essentially every analyzed element subjected to a temperature gradient has developed the same fractionation behavior and generally scales with mass/atomic number (Bindeman et al., 2103; Richter et al., 2008; Huang et al., 2009; Huang et al., 2010; Lacks et al., 2012). Temperature gradient driven isotopic fractionation is therefore a viable candidate for producing the Fe isotope trends observed at Torres del Paine and other felsic plutons. If a downward moving steady-state temperature gradient moved through the Torres del Paine pluton during emplacement, the Fe isotope fractionation trend could potentially be reproduced.

Lundstrom (2009) proposed an alternative mechanism for granitoid formation which explains how temperature gradients can create the observed compositional differentiation and isotopic fractionation in zoned convergent margin plutons (Figure 17). Thermal Migration Zone Refining (TMZR) combines the idea of top-down incremental pluton emplacement with in situ temperature gradient driven compositional differentiation. The in situ process is illustrated by

laboratory experiments which show that andesite containing 4 wt.% water in a temperature gradient can self-differentiate with granite forming at the cold end of the gradient (Huang et al., 2009). Thus, as a pluton grows downward during TMZR, a steady-state temperature gradient is established between the older colder sills at the top of the intrusion and the warm underplating sills. The temperature gradient drives compositional differentiation by diffusive transport of components with mineral-melt equilibrium dictated by the local temperature; this process is called thermal migration. As warm sills continue to accumulate below the growing pluton, the temperature gradient moves down through the system. This downward moving process enriches the cold top of the pluton in low temperatures phases (quartz, orthoclase); the warm base of the pluton is enriched in high temperature mafic phases leaving behind a wake of differentiated granitoid. The end product of TMZR is a zoned convergent margin pluton with granitic rocks at the top of the intrusion and mafic rocks at the base of the intrusion.

TMZR will also produce predictable temperature gradient stable isotope fractionation patterns (Figure 18) (Lundstrom 2009). The same temperature gradient effect that drives the cold margins of the pluton toward more felsic compositions will also drive heavy isotope enrichment toward the cold margins of the pluton. A downward moving temperature gradient should therefore produce a spatially dependent Fe isotope profile within the pluton where δ^{56}Fe decreases with depth in the pluton. The model predicts (1) that granites at the cold margins of the pluton will be isotopically heaviest. (2) The granites lower in the intrusion will have intermediate isotopic values. (3) The warm mafic root of the pluton should be isotopically lightest (Lundstrom, 2009). Thus, temperature gradient driven fractionation can be directly tested by analyzing Fe isotopes along well-defined vertical and horizontal transects in zoned convergent margin plutons.

Temperature gradient isotope fractionation at Torres del Paine

The Torres del Paine pluton contains all of the necessary parameters to test the TMZR model. Specifically, the Torres del Paine pluton is a zoned convergent margin related pluton, its geochronology is consistent with an incremental top-down pluton emplacement process and its exposure allows for detailed spatial sampling of the pluton with respect to its margins. Our Fe isotope data are consistent with the isotopic stratification with position predicted by temperature gradient fractionation as outlined in the TMZR model. Specifically, the marginal granites are isotopically heavier compared to the interior granites, and the diorites and gabbros of the underlying PMC have the isotopically lightest Fe isotope values of the intrusion (Figure 12).

The most compelling evidence for temperature gradient isotope fractionation at Torres del Paine is the decrease in $\delta^{56}Fe$ from the granites at the margins of the pluton (within 800 meters of the country rock contact) to the granites in the interior of the pluton (granites within 100 meters of the PMC). Granites from the Valle Torres and Valle Silencio country rock/granite transects have an average Fe isotope value of +0.25 ± 0.02 2se. This is 0.08 per mil heavier than granites located in the interior of the pluton. The TMZR model predicts that granites at the top margins of the intrusion should have the heaviest isotopic values. This is because the granites at the top of the intrusion represent the oldest and coldest region of the pluton. The first melts injected into the upper crust quickly lose their heat to the surrounding country rock. As new melts underplate, a steady state temperature gradient is established between the cold margin of the pluton and the new warm melts (Figure 17). This temperature difference fractionates Fe such that the cold margins of the pluton become isotopically heavy and the underplating melts become isotopically light. The large available pool of heavy Fe becomes enriched in the marginal Torres del Paine granite and creates the isotopically heaviest region of the pluton.

As new warm melts incrementally underplate the growing pluton, the temperature gradient moves down through the system. Heavy Fe isotope enrichment continues to occur at the cold end of the gradient, but now it occurs lower within the growing pluton. At depth, however, the available pool of heavy Fe is substantially smaller because this area of the pluton was subject to the warm end of the gradient (light isotope enrichment) at an earlier time in the process. In other words, enrichment along the cold end of the gradient at lower depths in the pluton will drive heavy isotope enrichment, but the heavy isotope enrichment process will be much smaller in magnitude because it is acting on a material with light isotope enrichment from an earlier time. Temperature gradient driven differentiation would therefore produce an intermediate isotopic composition ($\delta^{56}Fe$= +0.17 ± 0.02 2se) in the interior Torres del Paine granites. Of the four assessed fractionation mechanisms in this discussion, only temperature gradient driven fractionation can explain the isotopic variation between the marginal and interior Torres del Paine granite. The combination of the top-down pluton at Torres del Paine as suggested by with Michel (2008) and a downward moving temperature gradient can explain the spatial variation of Fe isotope ratios in the Torres del Paine granite.

The second major observation consistent with temperature gradient induced isotope fractionation is the isotopically light region of diorites and grabbros in the underlying PMC. $\delta^{56}Fe$ values of diorites and gabbros throughout the unit are substantially lower ($\delta^{56}Fe$= +0.11 ± 0.02 2s.e) compared to the two overlying granitic units. The samples collected along the vertical Castillo

transect show fairly homogenous isotopic values that deviate little from mafic earth values (Poitrasson et al., 2004). The TMZR model predicts that the diorites and gabbros of the mafic root of a zoned convergent margin pluton should have the lightest isotopic signatures. This is because the downward moving temperature gradient has effectively enriched the warm insolated base of the pluton in isotopically light Fe.

In summary, we highlight the major observations that support temperature gradient driven Fe isotope fractionation at Torres del Paine. The downward moving temperature gradient model connects the top-down incremental assembly of the pluton suggested by Michel et al. (2008) and Leuthold et al. (2012) with the spatial variations of Fe isotopes observed in Torres del Paine. First, the decrease in δ^{56}Fe from the marginal granites to the mafic root is consistent with the predicted temperature gradient fractionation pattern outlined in the TMZR model (Lundstrom, 2009). Second, temperature gradient fractionation is the only known mechanism able to produce the isotopic variation between the marginal and interior Torres del Paine granite. This new evidence for temperature gradient fractionation at Torres del Paine has large implications on how magmas differentiate and how plutons are emplaced into the shallow crust.

Differentiation of the Torres del Paine Pluton via TMZR

The origin of the Torres del Paine pluton is previously attributed to the injection of multiple pulses of granitic melt into the existing Cerro Toro formation followed by the injection of a series of mafic sills at the base of the granite (Michael, 1991, 1984; Michel et al., 2008; Leuthold et al., 2012). High resolution dating of the intrusion support this idea and give clear evidence that the Torres del Paine pluton was emplaced top-down over the course of 160ky (Michel et al., 2008; Leuthold et al., 2012). This incremental emplacement mechanism operates on realistic geophysical constraints of magma emplacement in the upper continental crust by taking into account upper crustal deformation rates and plutonic conductive cooling rates (Glazner et al., 2004). Yet, there still remains a large disconnect between incremental pluton assembly and how felsic melts are produced.

Here we propose an alternative model for the formation of the Torres del Paine pluton using temperature gradient differentiation in attempt to bridge the gap between incremental pluton emplacement and magmatic differentiation (Figure 17). The process begins with water rich subduction creating andesite melts that pond in the shallow crust (Taylor 1965). Successive underplating of new andesite magma creates a temperature gradient between the warm arriving magma and cool preexisting melt. As sills continue to accumulate, the pluton grows downward at

the rate of vertical addition of magma. We assume a 15mm/yr emplacement rate (consistent with crustal deformation rates) for Torres del Paine in order to create the 160ky age difference found between the oldest granites and youngest mafic unit (Leuthold et al., 2012). This addition of melt leads to a near steady state downward moving temperature gradient. The temperature gradient induces wet thermal migration which transports mafic components toward the hotter region (newly injected sill) and silicic components toward the cool end of the gradient in the mush overlying the sill injection. As this refining zone proceeds downward, it leaves behind a differentiated granitoid with the Torres del Paine granite located at the top of the intrusion and the PMC located at the base of the pluton.

The compositional change produced by temperature gradient differentiation can be modeled using IRIDIUM a diffusive transport thermodynamic modeling program (Boudreau, 2003). Stacking successive sills of andesite in a 300 degree temperature gradient over 160kys creates SiO_2 enrichment at the top of the pluton and MgO enrichment at the base of the pluton (Figure 19). Importantly, these model results indicate that TMZR can reproduce the compositional zoning observed at Torres del Paine. Moreover, the compositional differentiation via TMZR occurs in situ and does not require melting from a preexisting felsic mineral assemblage to produce silicic granite. The model also fits within the framework of reasonable geophysical pluton emplacement constraints.

Conclusion

In this study we have presented new Fe isotope data for the zoned convergent margin-related Torres del Paine pluton. Our data show a spatially controlled distribution of Fe isotopes in the pluton with high δ^{56}Fe values in the marginal granites, intermediate δ^{56}Fe values in the interior granites and low δ^{56}Fe values in the mafic base of the pluton. We assessed these results in the context of four fractionation mechanisms: crustal assimilation, fractional crystallization, late stage fluid exsolution and temperature gradient driven differentiation. Of these four mechanisms, only temperature gradient differentiation explains the spatial variations in Fe isotopes observed in the pluton. The temperature gradient differentiation model is consistent with both the compositional zonation and age variations observed in the Torres del Paine pluton. The model is also consistent with geophysically reasonable crustal deformation and conductive cooling rates. Finally, we presented a new temperature gradient differentiation based model for the formation of the Torres del Paine pluton. Fe isotope data and thermodynamic modeling strongly support the idea that the Torres del Paine pluton was formed by a temperature gradient differentiation process.

Figures

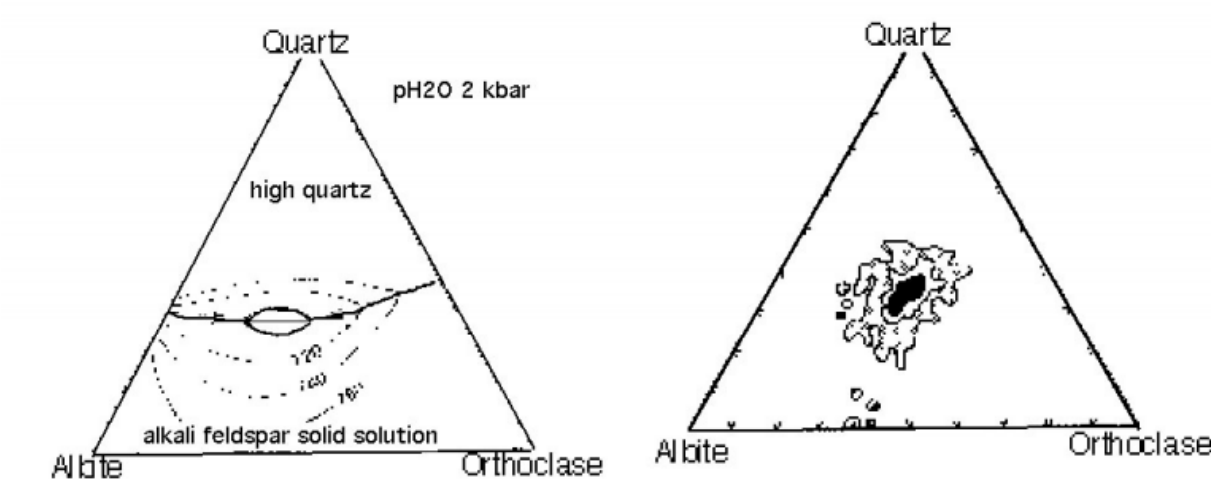

Figure 1

Ternary diagram of the $NaAlSi_3O_8$-$KAlSi_3O_8$-SiO_2-H_2O system showing the experimentally determined granite minimum melt (left diagram) (Tuttle and Bowen 1958). Granites and rhyolites from around the world plot along the experimentally determined quartz-feldspar minimum melt composition (right diagram). This diagram implies that granite formation is thermodynamically controlled and that granites are igneous in origin.

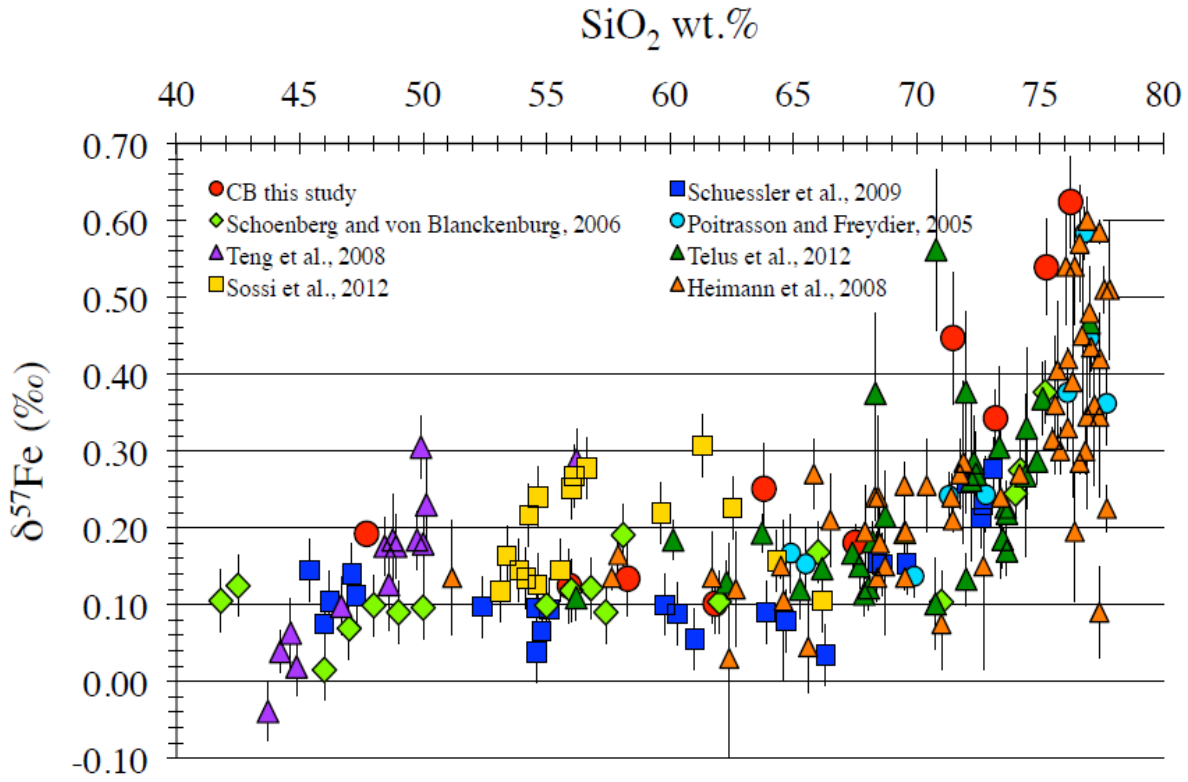

Figure 2

Studies show an increase in $\delta^{57}Fe$ with increasing SiO_2 in both plutonic and volcanic systems. The process responsible for Fe isotope variations in igneous rocks remains largely unknown and debated.

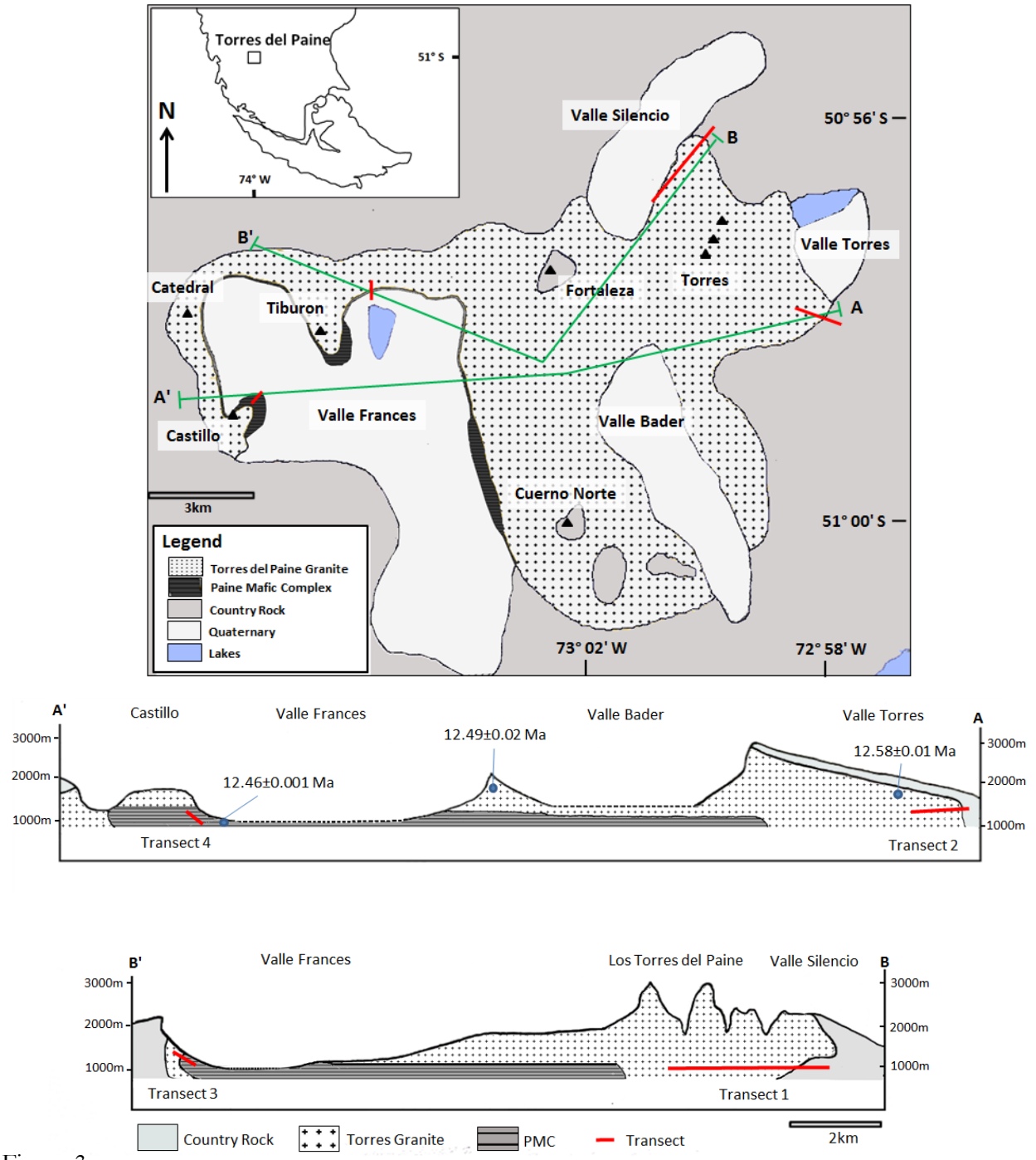

Figure 3

Geologic map of the Torres del Paine pluton (upper diagram). Note cross section traces A-A' and B-B' (lower diagram). No vertical exaggeration. The nature of the PMC in the eastern part of the pluton is inferred as no PMC outcrops exist in this region. Dashed lines along the talus covered valley floors also indicate inferred geology. Age dates were taken from Leuthold et al. (2012). The pluton becomes younger with depth. Marginal granites are the oldest (12.58 ± 0.02 Ma), interior granites are younger (12.49 ± 0.02 Ma) and diorites and gabbros of the PMC are the youngest (12.46 ± 0.001 Ma). Samples were collected along the transects highlighted in red.

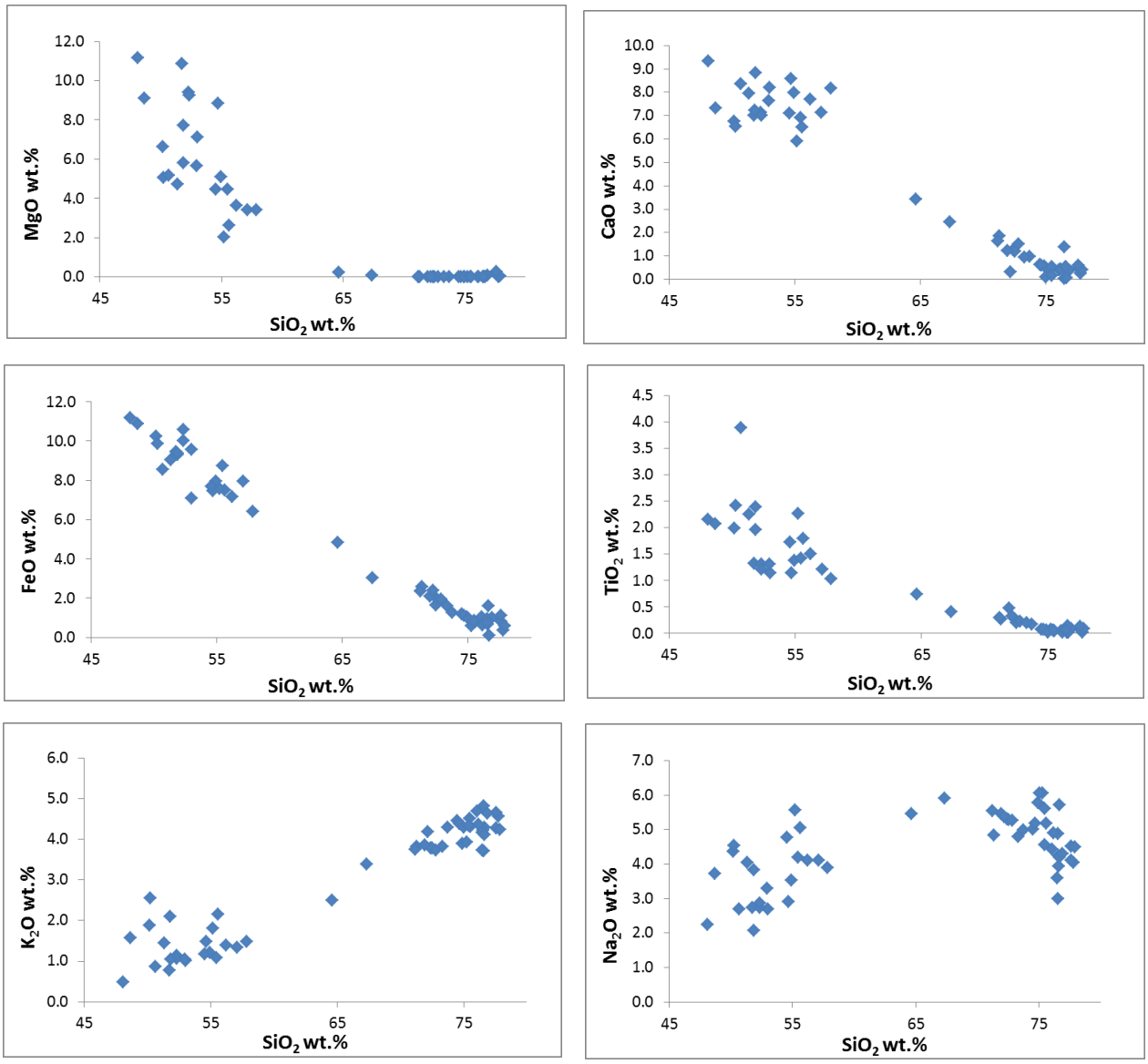

Figure 4

Harker plots of Torres del Paine data suggest a genetic relationship between the Torres del Paine granite and the underlying PMC.

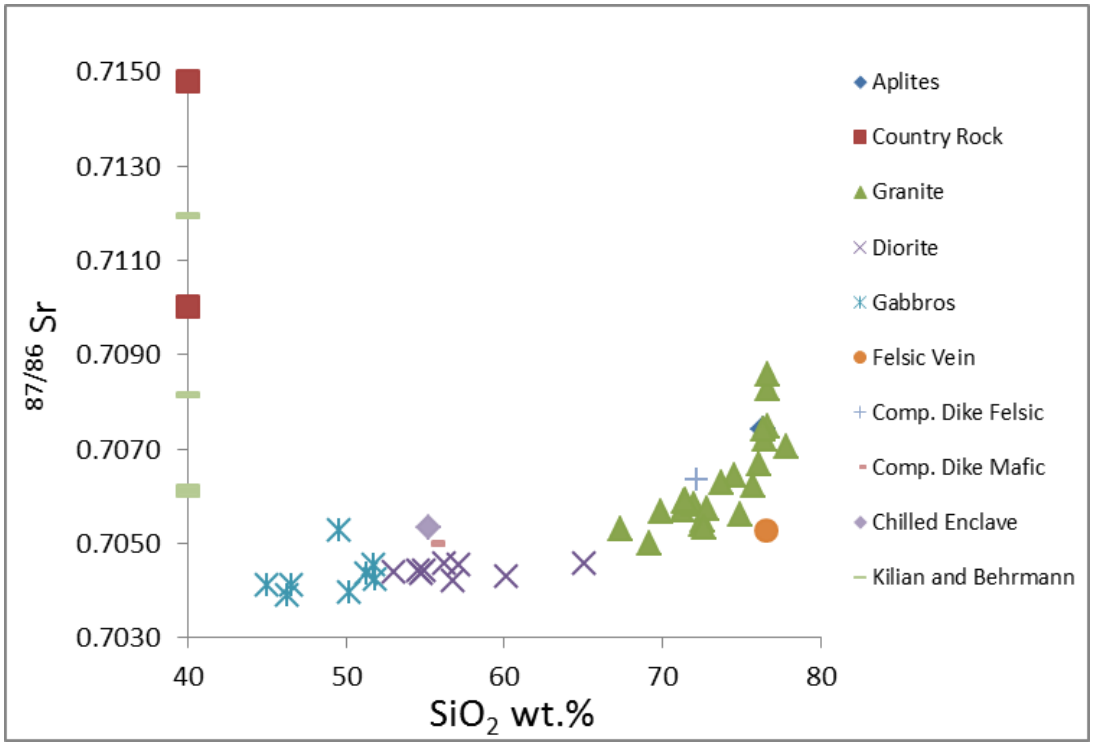

Figure 5

Sr isotope data for the sample set increases with increasing SiO_2. The Cerro Toro formation country rock is notably very radiogenic. Sr isotope values for nearby Chilean trench sediments (Kilian and Behrmann, 2003) overlap with Torres del Paine sample set values.

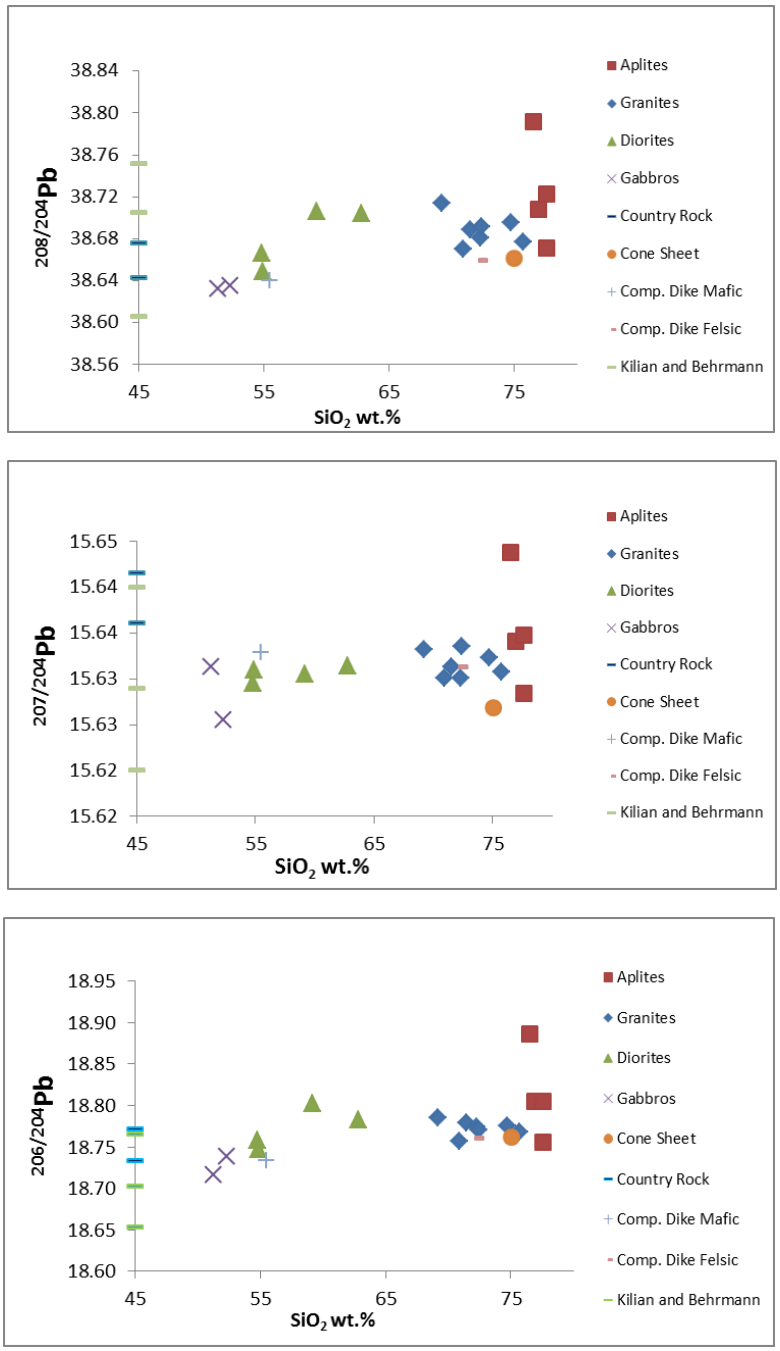

Figure 6

Pb isotope data for the Torres del Paine data set. Granite, diorites and gabbros from Torres del Paine data have an average $^{208}Pb/^{204}Pb$= 38.68+/- 0.06, $^{207}Pb/^{204}Pb$= 15.63+/- 0.01 and $^{206}Pb/^{204}Pb$= 18.77+/- 0.06. Aplite samples were age corrected. The Cerro Toro country rock has $^{208}Pb/^{204}Pb$= 38.66+/- 0.03, $^{207}Pb/^{204}Pb$= 15.64+/- 0.01 and $^{206}Pb/^{204}Pb$= 18.75+/- 0.04. Pb isotope values for the nearby Chilean trench sedimentary samples (Kilian Behrmann, 2003) overlap with Torres data.

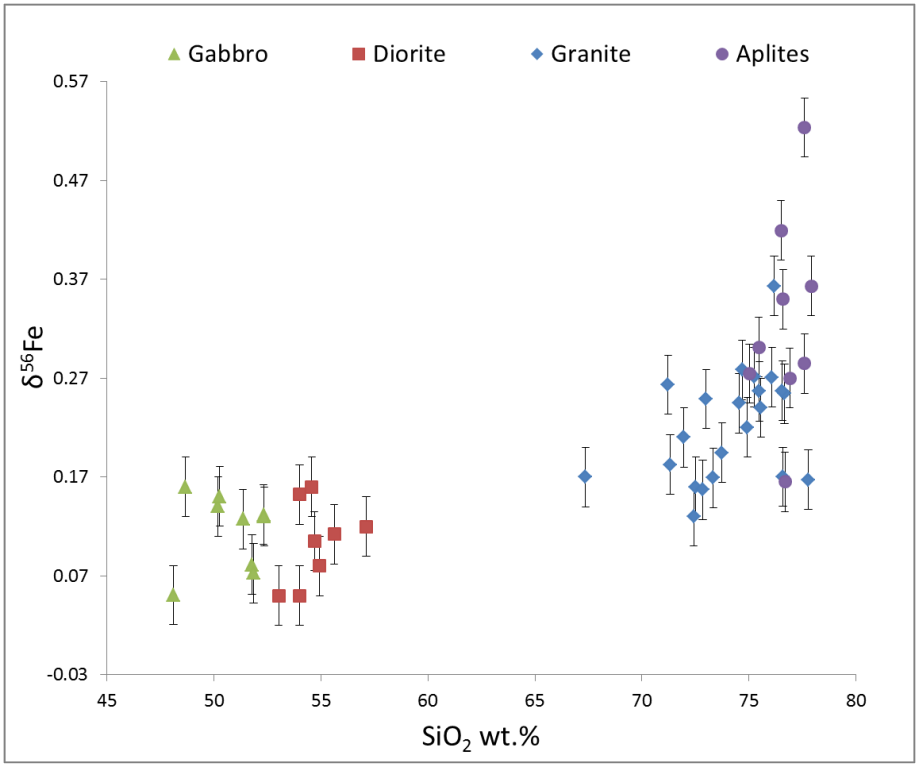

Figure 7

Torres del Paine samples agree with previously observed Fe isotope trends. Granites and aplites are isotopically heavy. Gabbros and diorites have mean mafic earth values (Poitrasson et al., 2004).

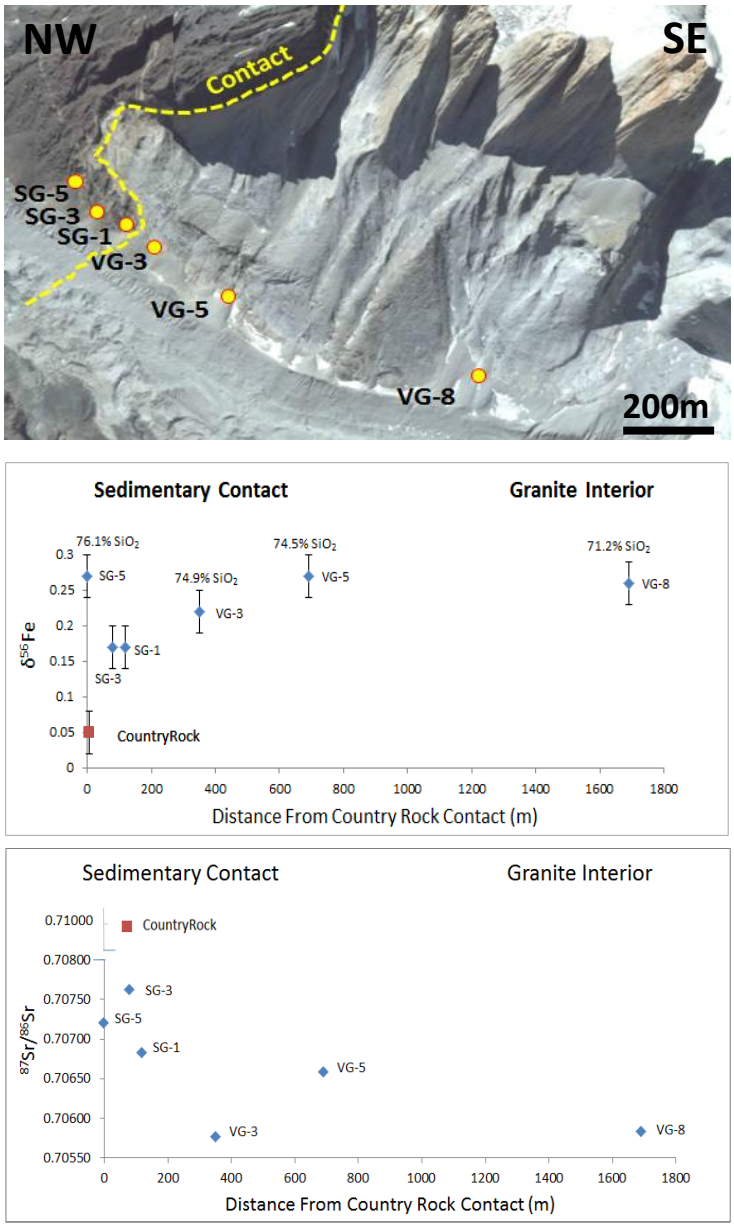

Figure 8

Satellite image of the Valle Silencio country rock/granite transect with sample names and locations (upper diagram). Fe and Sr data for the Valle Silencio country rock/granite transect (lower diagrams). δ^{56}Fe for average marginal granites is δ^{56}Fe= +0.25 ± 0.02 2se. Sample SG-3 and SG-1 taken from granite pods within the country rock near the country rock/granite contact exhibit isotopically lower δ^{56}Fe values compared to average granite isotopic values. These samples are also higher in radiogenic Sr compared to average granite samples. The low δ^{56}Fe and high $^{87/86}$Sr ratio of these samples likely corresponds to assimilation of low δ^{56}Fe and high $^{87/86}$Sr country rock. SiO_2 content also increases toward the margin of the pluton. The country rock value is an average of two mudstone samples (Gt-Xtry and LA) taken from other places in the massif (Valle Silencio and Laguna Armaga park station).

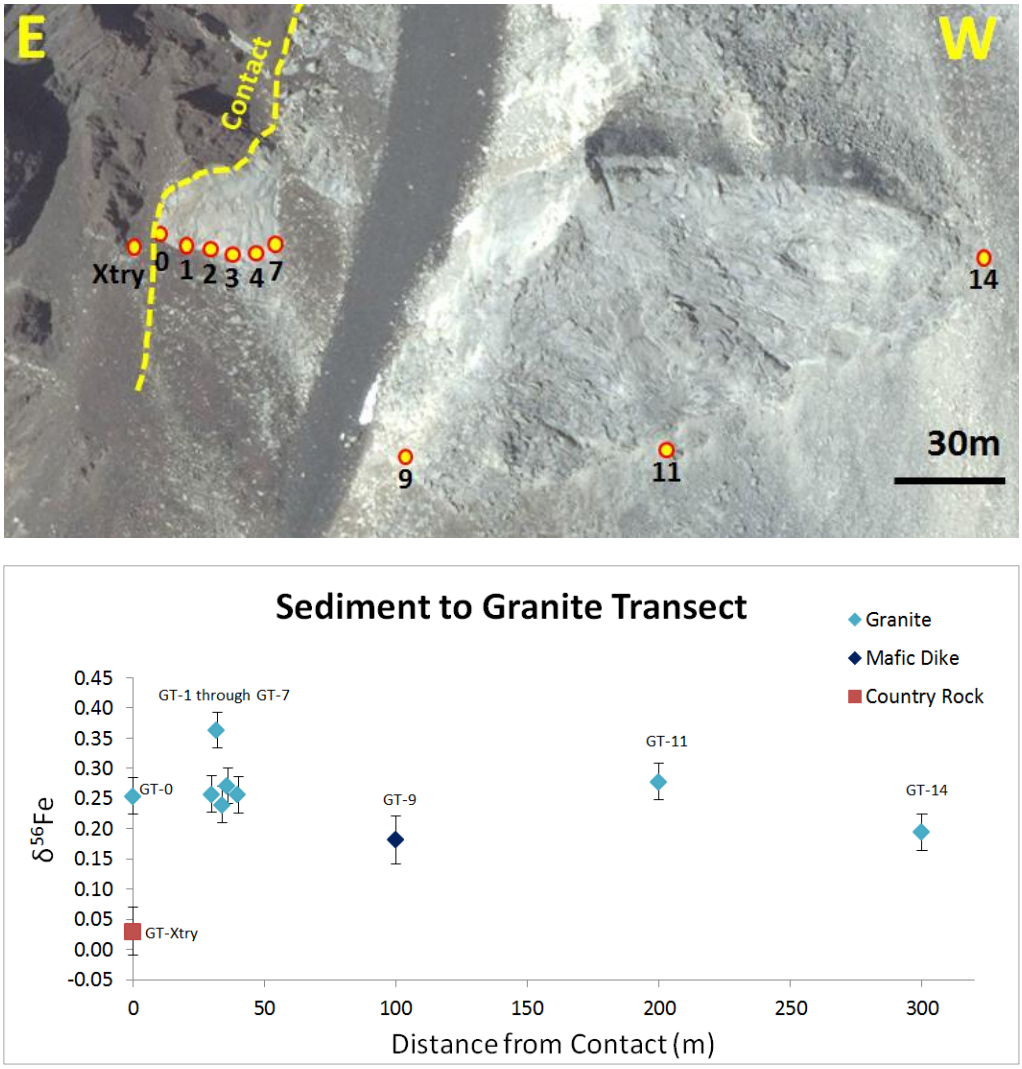

Figure 9

Satellite image of the Valle Torres country rock/granite transect with sample names and locations (upper diagram). Fe isotope data for the Valle Torres country rock/granite transect (lower diagram). δ^{56}Fe for average marginal granites is δ^{56}Fe= +0.25 ± 0.02 2se. Country rock sample Gt-Xtry is isotopically light (δ^{56}Fe= +0.03 ± 0.05‰).

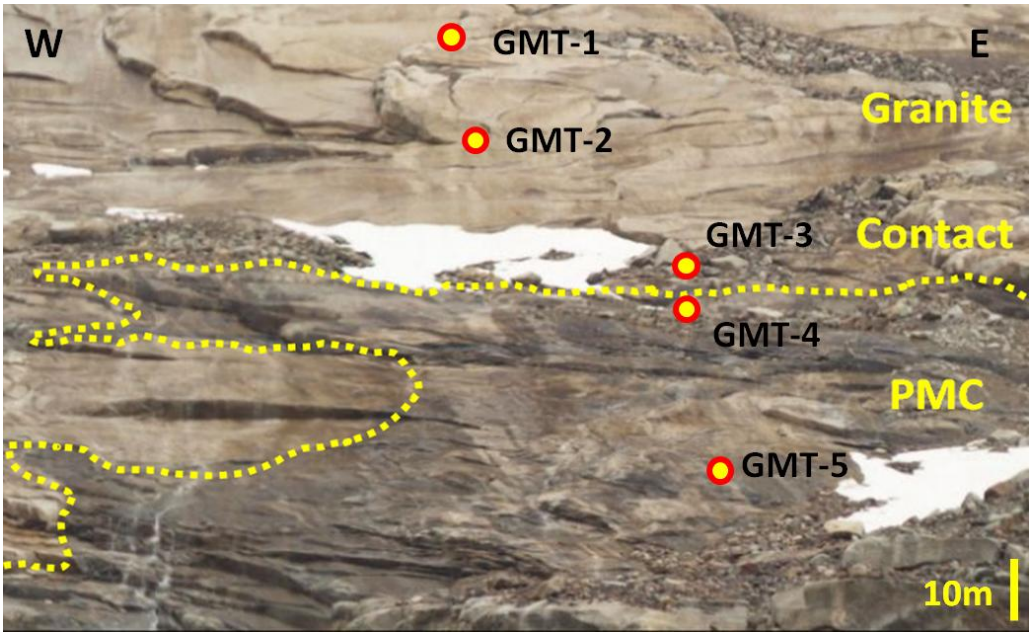

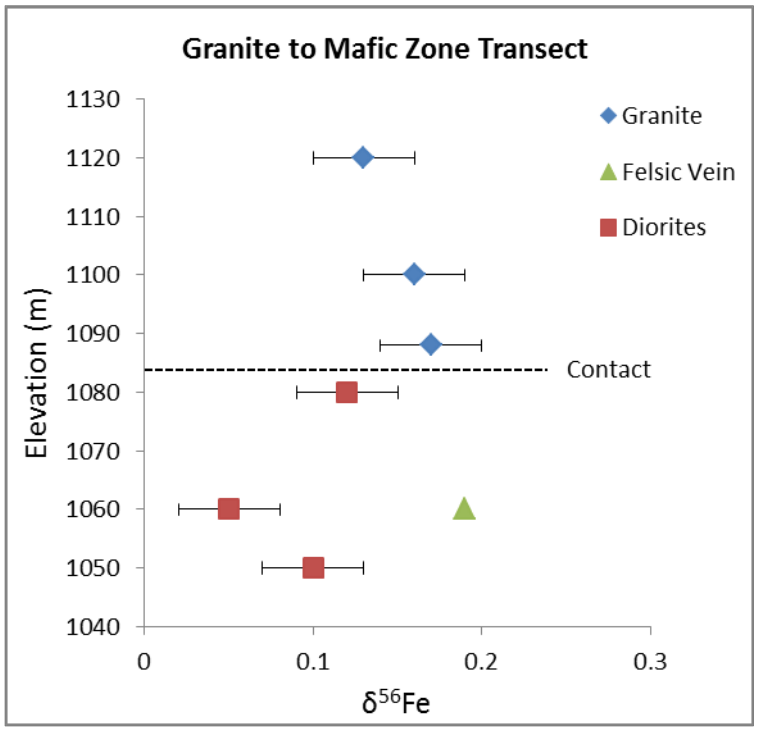

Figure 10

Representative photo of the Northern Wall of the Valle Frances granite/ PMC transect (upper diagram). The 100m vertical transect starts in the homogenous granite (three samples) and moves into the diorite sills of the PMC (four samples). The three granite samples show below average $\delta^{56}Fe$ granite values ($\delta^{56}Fe$= +0.15 ± 0.03‰) (lower diagram). The underlying diorites are within mean mafic earth isotopic values (Poitrasson et al., 2004). A 2cm wide felsic vein running through diorite sills has $\delta^{56}Fe$ values of +0.19 ± 0.03‰.

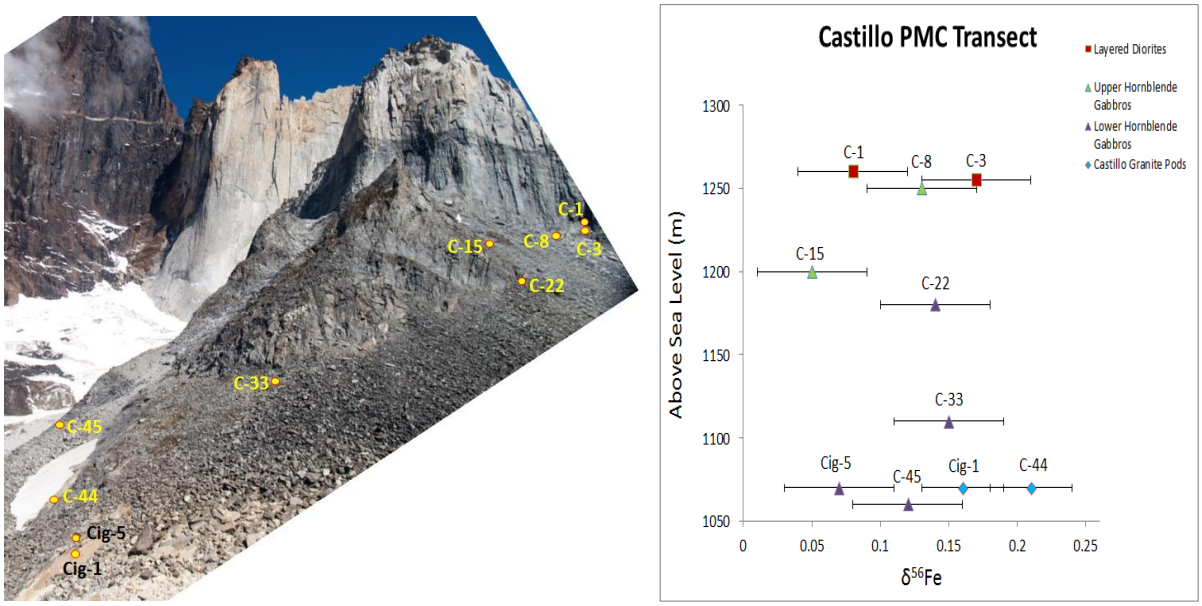

Figure 11

Photograph image of the vertical Castillo PMC transect with sample names and locations (left diagram). The layered diorite, upper hornblende gabbros and lower hornblende gabbros exhibit homogenous Fe isotope values that deviate little from mean mafic earth values (Poitrasson et al., 2004). Granite pods at the base of Castillo have isotopically lighter values ($\delta^{56}Fe = +0.18 \pm 0.03‰$) compared to marginal granites (right diagram).

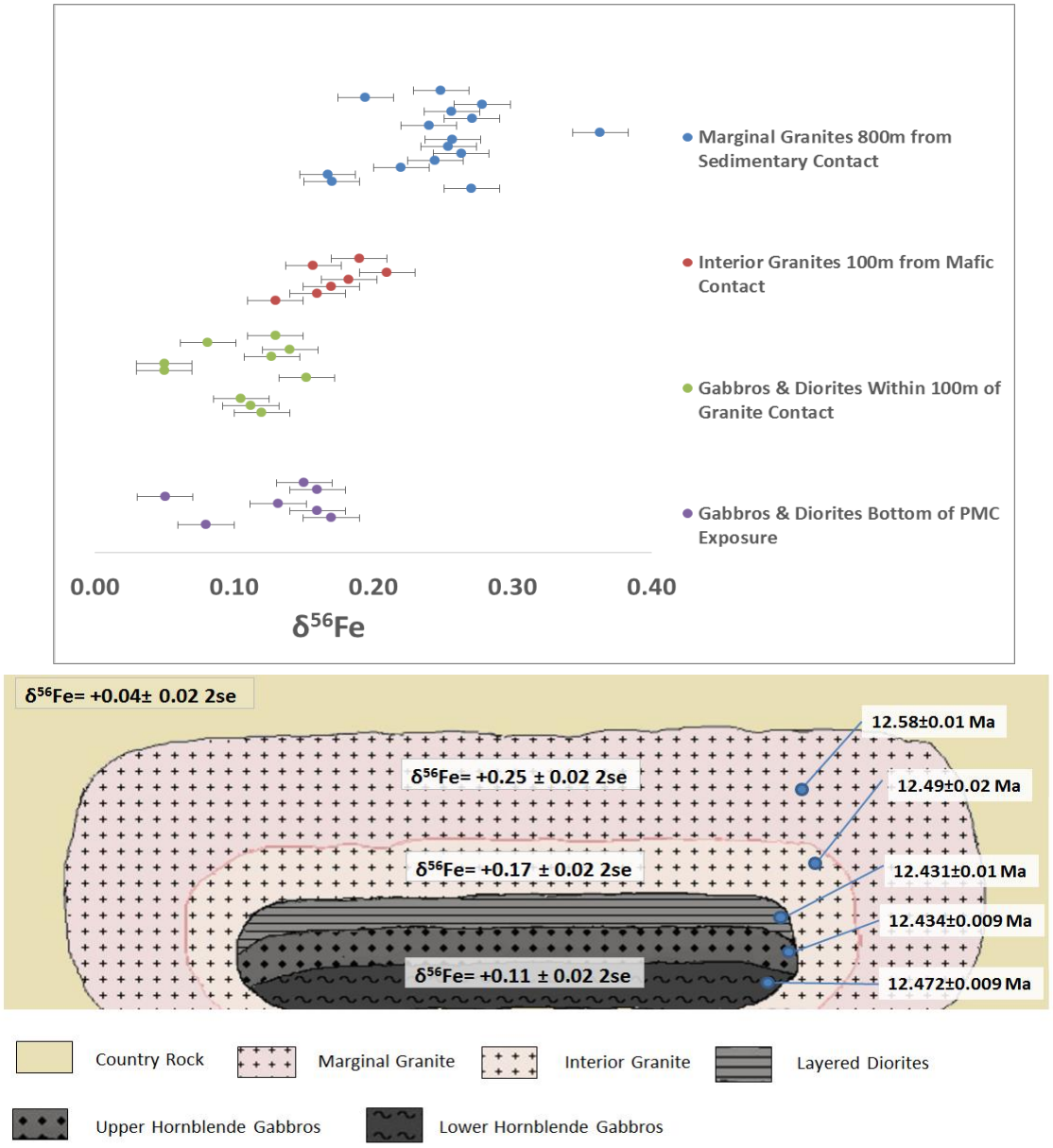

Figure 12

Fe isotope data from Torres del Paine reveals a spatially dependent Fe isotope trend in the intrusion (upper diagram). Specifically, isotopic values increase in δ^{56}Fe away from the mafic base of the intrusion. Granite samples within 800 meters of the country rock/granite contact are isotopically heaviest (average δ^{56}Fe= +0.25 ± 0.02 2se). Interior granites within 100 meters from the underlying PMC are intermediate in isotopic value (average δ^{56}Fe= +0.17 ± 0.02 2se). Gabbro and diorites in the underlying PMC have the lowest δ^{56}Fe values, and are largely homogenous and within mean mafic earth values (Poitrasson et al., 2004). Average Fe isotope values and age dates (Michel et al., 2008; Leuthold et al., 2012) for each region are illustrated in a cartoon of the Torres del Paine pluton (lower diagram).

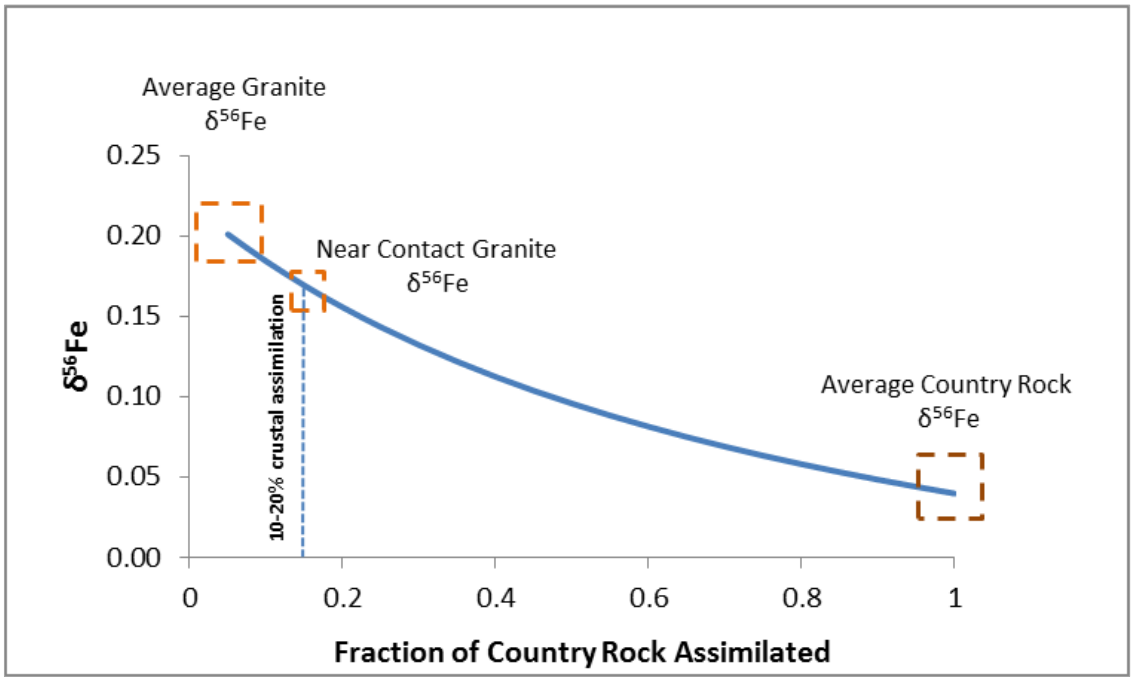

Figure 13

Mixing model between average granite $\delta^{56}Fe$ values and average country rock $\delta^{56}Fe$ values. The model follows the mixing equation $\delta^{56}Fe_{mix} = (f_1\delta_1C_1+f_2\delta_2C_2)/(f_1C_1+f_2C_2)$; where, f_1 is fraction of granite, f_2 is fraction of country rock, δ_1 is average granite $\delta^{56}Fe$ ($\delta^{56}Fe = +0.22$), δ_2 is average country rock $\delta^{56}Fe$ ($\delta^{56}Fe = +0.04$), C_1 is Fe concentration of granite (1.35%), C_2 is Fe concentration of country rock (3%).10-20% assimilation can explain the isotopically lighter values ($\delta^{56}Fe = +0.17 \pm 0.04$) in granite pods located in the country rock near the country rock/granite contact. The mixing model indicates 10-20% crustal assimilation to produce the lower near margin granite values.

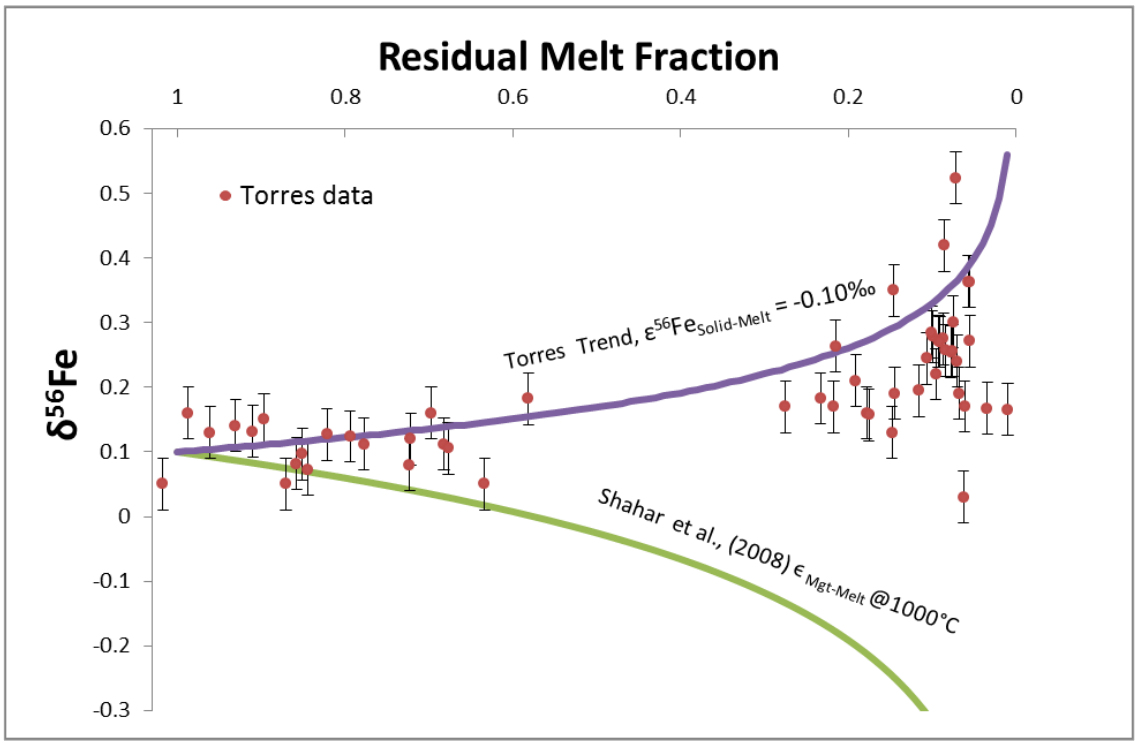

Figure 14

Rayleigh Distillation curve comparing the observed Torres del Paine fractionation trend with the experimentally predicted magnetite-melt fractionation trend. The residual melt fraction corresponds to FeO/FeO initial; in this scenario FeO initial is 10 wt.%. The best fit fractionation factor for solid vs. melt for Torres del Paine data is -0.10‰ ($\varepsilon = 1000 \ln \alpha$); it is illustrated using the purple line. The green line represents a Rayleigh distillation using the experimentally determined Shahar et al. (2008) magnetite-fayalite fractionation factor ($\varepsilon_{Mgt\text{-}Melt}$ is 0.18‰ for a T= 1000°C). The model shows that crystallizing magnetite from melt via a Rayleigh distillation process should leave the residual melt isotopically light. This is the opposite of what is observed in the Torres del Paine data trend and felsic plutons in general. The lack of overlap between these two curves argues against a fractional crystallization mechanism.

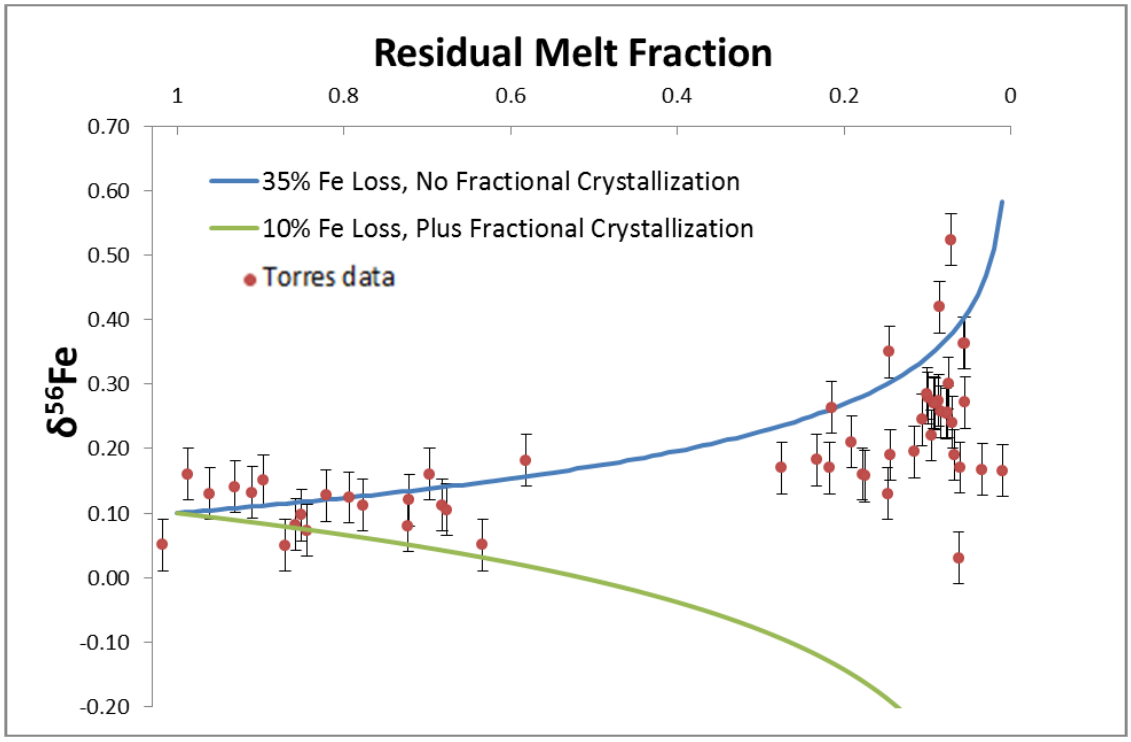

Figure 15

Rayleigh distillation plot comparing various Fe isotope fractionation factors associated with removing an Fe bearing fluid in equilibrium with magma containing magnetite. Equilibrium fluid magnetite experiments reveal that removal of a fluid could produce isotopically heavy granites: $\epsilon_{fluid\text{-}magnetite}$ ~-0.30‰ at 800°C (Bilenker et al., 2013). However, the fluid removal requires unreasonable amounts of Fe loss to produce the fractionation trend observed at Torres del Paine. The blue line assumes 35% of the Fe is removed from the granites via a fluid. The blue trend reproduces the Torres del Paine trend; however, it neglects any isotopic fractionation caused by fractional crystallization. The green line represents a more realistic circumstance where 10% of the Fe in the system is removed via fluid loss and the remainder of the Fe is removed via fractional crystallization. This green fractionation line, however, does not reproduce the Torres trend.

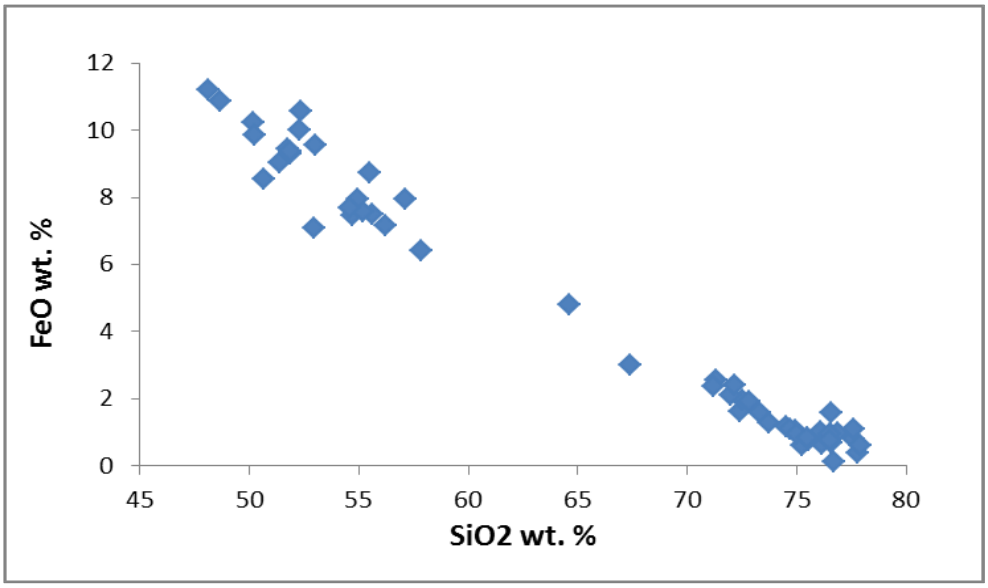

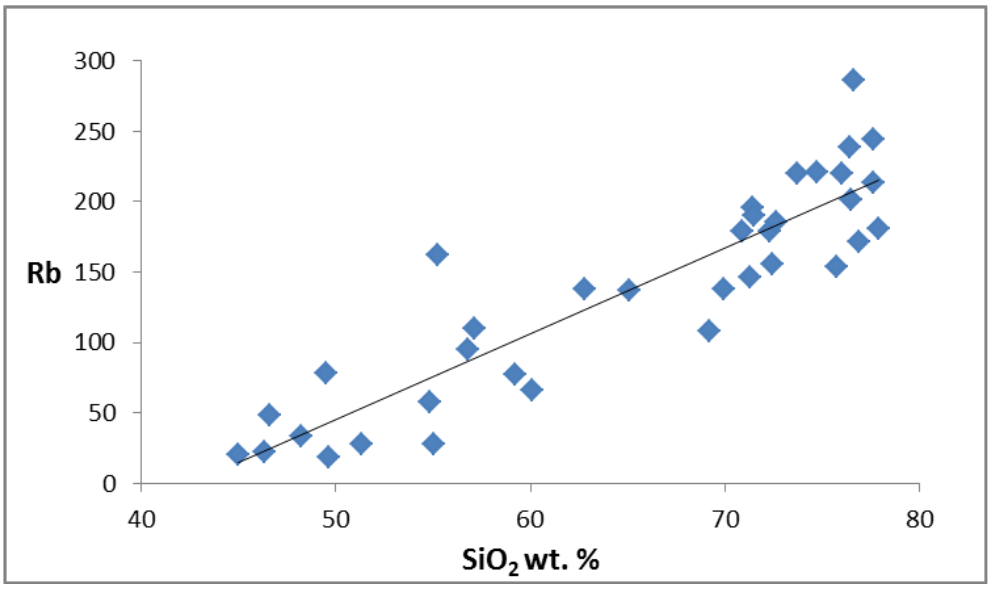

Figure 16

Harker plot of SiO_2 vs FeO reveal a normal differentiation trend (upper diagram). The plot indicates that weight percent levels of Fe are not likely removed by fluid loss. Plots of fluid mobile Rb vs SiO_2 also reveal normal differentiation trends, suggesting that significant amounts of fluid loss did not affect the Torres del Paine pluton (lower diagram).

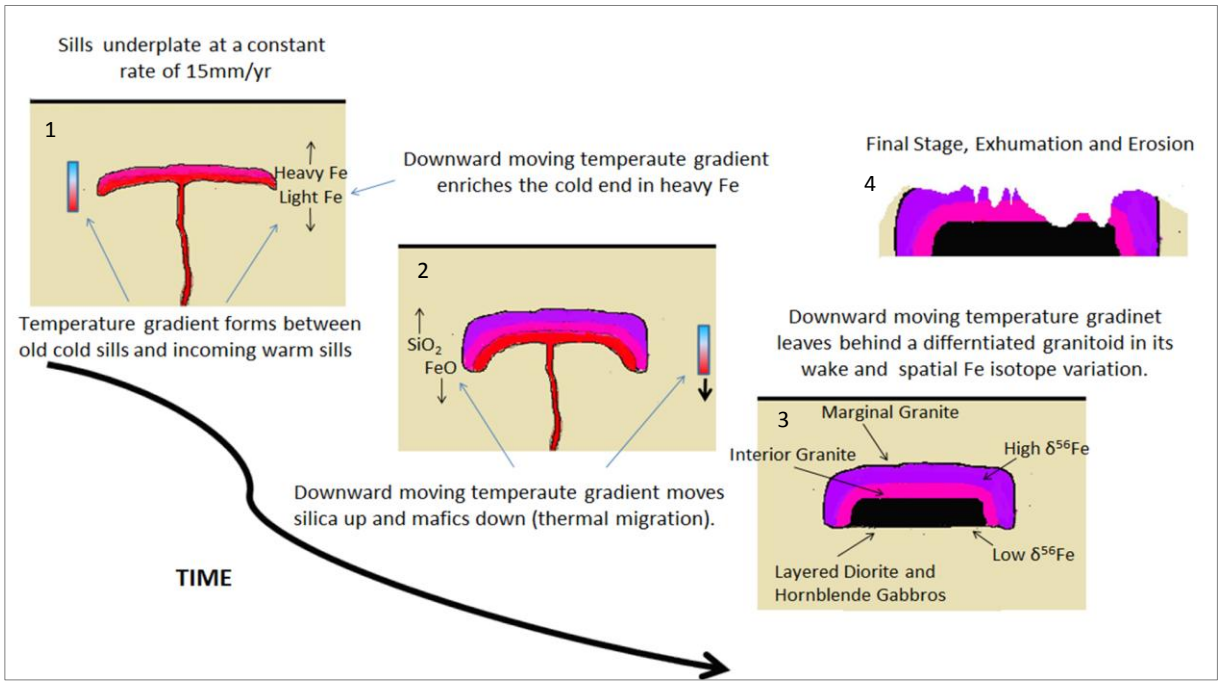

Figure 17

We present an alternative model for the formation of the Torres del Paine pluton. Panel 1 shows subduction related magmas ponding in the shallow crust at a rate of 15 mm/yr. A temperature gradient is established between the older cold sills at the top of the intrusion and the warm arriving magma. The temperature gradient fractionates Fe such that heavy Fe is enriched at the cold end of the gradient. As successive magmas underplate the intrusion, the downward moving temperature gradient moves silica up toward the cold end of the system and mafic phases down to the warm end of the system; this process is thermal migration (Panel 2). The final product of this process is a zoned pluton with granite at the top of the intrusion and diorites and gabbros at the base of the intrusion (Panel 3). Fe isotope variation is preserved spatially in the pluton with the granites at the top of the intrusion exhibiting high δ^{56}Fe values; the diorites and gabbros at the base of the intrusion exhibiting low δ^{56}Fe values. Subsequent uplift and erosion produces the present day topography we observe at Torres del Paine (Panel 4).

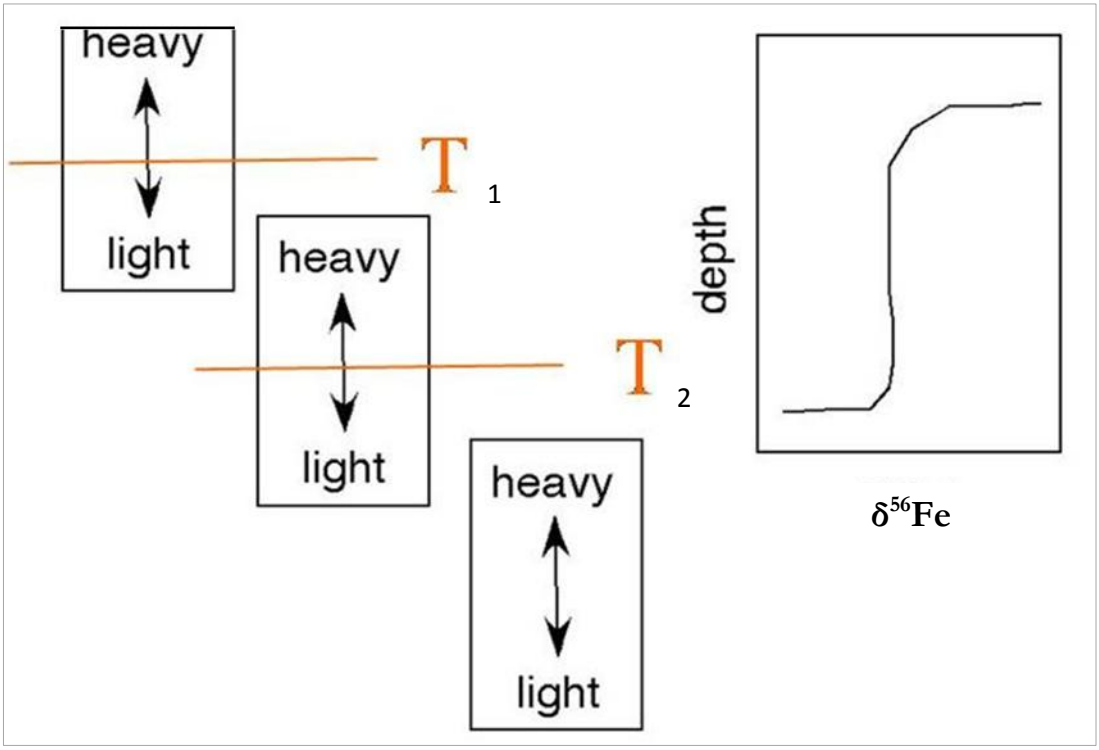

Figure 18

When a temperature gradient is established in a growing pluton, heavy isotopes are enriched at the cold end of the gradient and light isotopes are enriched at the warm end of the gradient. As the temperature gradient moves down through the system from T_1 to T_2 it leaves behind an S-shaped isotopic profile where $\delta^{56}Fe$ decreases with depth in the intrusion. A downward moving temperature gradient process will therefore leave the rocks at the top of the intrusion isotopically heavy and rocks at the base of the intrusion isotopically light. Rocks in the middle of the intrusion will have intermediate isotopic values.

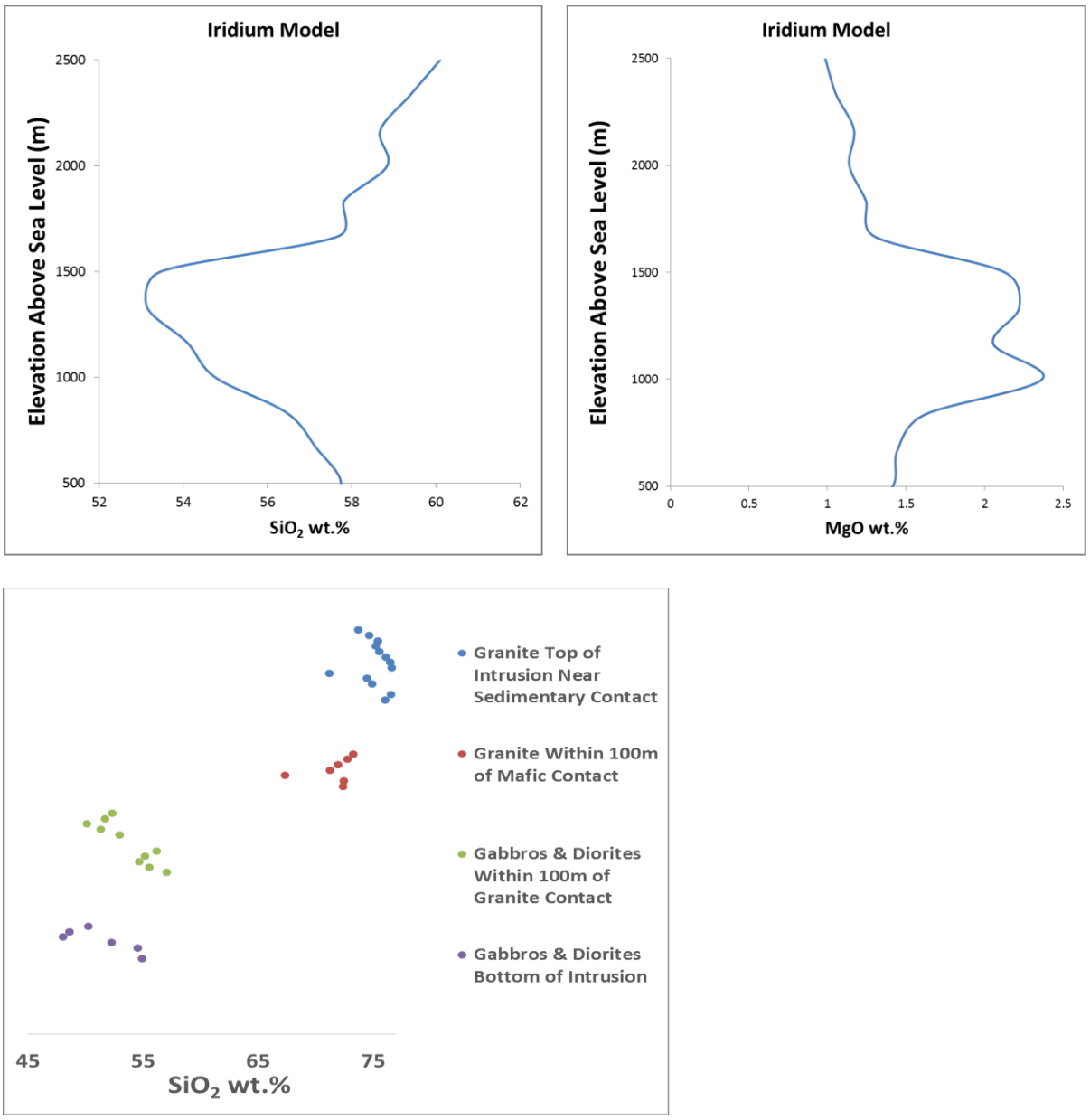

Figure 19

Compositional modeling of temperature gradient driven differentiation using IRIDIUM (a diffusive transport thermodynamic modeling program) (Boudreau, 2003). Stacking successive sills of andesite in a 300 degree temperature gradient over 160kys creates SiO_2 enrichment at the top of the pluton (upper left diagram) and MgO enrichment at the base of the pluton (upper right diagram). This zonation in components is consistent with what is observed in the zoned Torres del Paine pluton (lower diagram).

Tables

Granites		Al_2O_3	CaO	FeO	MgO	P_2O_5	K_2O	SiO_2	Na_2O	TiO_2	Rb
	GMT-1	14.75	1.27	1.62	0.00	0.58	3.79	72.42	5.31	0.26	
	GMT-2	14.72	1.18	1.96	0.00	0.36	3.78	72.52	5.29	0.19	
	GMT-3	17.35	2.45	3.02	0.09	0.03	3.39	67.37	5.90	0.41	
	VF-1	15.36	1.85	2.56	0.00	0.00	3.82	71.32	4.84	0.26	
	SG-5	13.33	0.41	1.02	0.00	0.00	4.70	76.08	4.42	0.04	
	SG-3	13.27	0.38	0.67	0.00	0.00	4.82	76.58	4.24	0.04	
	SG-1	12.92	0.24	0.37	0.00	0.09	4.56	77.77	4.04	0.02	
	VG-3	13.65	0.56	1.05	0.00	0.08	3.90	74.92	5.77	0.06	
	VG-5	14.13	0.64	1.17	0.00	0.00	4.46	74.53	5.00	0.06	
	VG-8	15.21	1.62	2.37	0.00	0.00	3.75	71.21	5.54	0.29	
	C-44	14.93	1.23	2.10	0.00	0.00	3.86	71.96	5.45	0.47	
	Cig-1	14.42	1.52	1.93	0.00	0.08	3.73	72.84	5.27	0.23	
	GT-0	13.42	0.50	0.86	0.00	0.00	4.30	76.66	4.20	0.06	
	GT-1	12.92	0.50	0.93	0.00	0.00	4.22	76.55	4.87	0.01	
	GT-2	13.37	0.43	0.63	0.00	0.12	4.37	76.17	4.90	0.02	
	GT-3	13.65	0.51	0.77	0.00	0.00	4.31	75.55	5.17	0.04	
	GT-4	13.70	0.40	0.60	0.00	0.00	3.92	75.25	6.06	0.07	
	GT-7	14.02	0.55	0.84	0.00	0.00	4.52	75.48	4.55	0.04	
	GT-11	14.02	0.59	1.10	0.00	0.00	4.39	74.68	5.17	0.06	
	GT-14	14.56	0.96	1.27	0.00	0.02	4.29	73.74	4.99	0.16	
	GT-15										
	ST-4	15.31	0.96	1.59	0.00	0.00	3.83	73.33	4.79	0.20	
	11_23	14.10	1.95	2.42	0.61	0.00	4.32	70.90	4.50	0.47	179
	10_10	14.10	2.20	2.38	0.51	0.02	7.05	69.20	3.96	0.38	108
	CF_3	14.90	1.75	2.51	0.47	0.11	4.35	69.90	4.19	0.38	138
	037-5	14.80	1.57	2.20	0.67	0.11	4.43	71.30	3.67	0.39	146
	1340C	14.20	1.65	2.43	0.42	0.14	4.28	71.40	4.26	0.40	196
	13-15	14.00	1.92	2.49	0.43	0.05	4.87	71.50	4.29	0.40	190

Table 1

Bulk Oxide and Rb concentrations for the Torres del Paine sample set.

		Al_2O_3	CaO	FeO	MgO	P_2O_5	K_2O	SiO_2	Na_2O	TiO_2	Rb
	1340C	14.20	1.65	2.43	0.42	0.14	4.28	71.40	4.26	0.40	196
	13-15	14.00	1.92	2.49	0.43	0.05	4.87	71.50	4.29	0.40	190
	039-A	14.30	1.45	2.58	0.55	0.09	4.59	72.30	4.30	0.34	179
	13_10	13.90	1.88	1.94	0.43	0.05	4.51	72.40	4.40	0.39	156
	CF-2	14.00	1.28	1.88	0.51	0.06	4.68	72.60	3.77	0.30	185
	10_20	13.10	1.32	1.70	0.11	0.00	4.96	73.70	4.21	0.12	220
	13_9	12.60	1.43	1.59	0.19	0.00	5.20	74.70	4.12	0.23	221
	038_6	13.60	0.64	1.37	0.23	0.04	4.74	75.70	4.12	0.20	154
	038_3	13.50	0.65	1.31	0.10	0.00	4.79	76.00	3.96	0.16	220
	038_2	12.80	0.59	1.29	0.26	0.01	4.68	76.40	4.47	0.13	239
Diorites											
	GMT-4	17.73	7.15	7.94	3.42	0.00	1.34	57.12	4.10	1.21	
	VF-2	18.35	6.50	7.50	2.63	0.40	2.15	55.62	5.04	1.80	
	VF-3	14.94	8.57	7.44	8.82	0.00	1.48	54.69	2.91	1.13	
	VF-6	18.68	5.90	7.59	2.03	0.96	1.80	55.20	5.57	2.26	
	VF-16	18.26	7.70	7.17	3.63	0.03	1.39	56.22	4.11	1.50	
	C-1	17.88	7.97	7.95	5.11	0.01	1.21	54.94	3.53	1.38	
	C-45	18.29	7.10	7.67	4.47	0.23	1.18	54.57	4.77	1.72	
	TB-1										
	TB-5										
	GMT-5M	17.24	8.21	9.57	7.11	0.00	1.00	53.02	2.70	1.14	
	P11-12	16.60	7.43	8.36	5.57	0.13	1.68	55.00	4.00	1.34	28
	P9-12	16.40	7.04	8.18	4.26	0.32	1.93	54.80	4.50	1.43	58
	P11-19	16.60	5.66	7.38	2.67	1.05	3.04	56.80	5.11	1.69	95
	P11-7	17.30	4.96	6.57	2.60	0.73	3.49	57.10	4.91	1.72	110
	P13-3	17.00	5.36	6.00	2.43	0.57	2.59	60.10	4.09	1.36	66
	O13-12a	16.80	5.33	5.97	2.65	0.46	2.61	59.20	4.56	1.29	77
	O13-12b	17.30	3.68	4.11	1.41	0.41	4.18	62.80	4.11	1.15	138
	T1200	15.20	3.44	4.75	1.45	0.42	3.57	65.10	4.71	0.78	137

Table 1 (cont.)

Bulk Oxide and Rb concentrations for the Torres del Paine sample set.

		Al_2O_3	CaO	FeO	MgO	P_2O_5	K_2O	SiO_2	Na_2O	TiO_2	Rb
Gabbros											
	VF-9	18.60	7.96	9.04	4.72	0.59	1.44	51.36	4.04	2.25	
	VF-11	17.33	6.75	10.23	6.63	0.64	1.88	50.20	4.36	1.98	
	VF-14	16.10	7.01	9.44	10.85	0.00	0.77	51.77	2.73	1.32	
	C-8	15.95	7.13	10.01	9.42	0.00	1.14	52.32	2.73	1.31	
	C-15	15.32	9.34	11.19	11.15	0.00	0.48	48.10	2.24	2.15	
	C-22	16.41	7.33	10.86	9.09	0.00	1.58	48.68	3.71	2.07	
	C-39	18.30	6.53	9.87	5.08	0.46	2.55	50.27	4.53	2.42	
	Cig-5	17.72	7.22	9.29	5.79	0.26	2.09	51.85	3.82	1.96	
	ST-5	15.61	7.02	10.57	9.26	0.05	1.06	52.35	2.87	1.21	
	P11-25	11.40	8.63	10.60	19.20	0.32	1.09	45.00	2.16	1.50	20
	P11-24	11.10	7.46	10.50	19.10	0.43	1.79	46.60	1.50	1.27	48
	O12-11	12.60	8.26	10.62	15.80	0.57	1.11	46.30	2.07	1.43	22
	P11-16	15.00	7.32	9.75	10.40	0.27	1.25	51.30	3.34	1.33	28
	P13-4	17.40	10.60	7.79	6.88	0.57	1.04	49.60	3.84	2.05	18
Aplites											
	10-19	12.50	0.46	0.79	0.14	0.00	4.28	77.60	4.52	0.07	213
	31-6	12.90	0.41	0.60	0.05		4.24	77.90	4.48	0.08	181
	9-16a	12.00	0.60	1.10	0.26	0.03	4.66	77.60	4.10	0.13	244
	9-11MC	12.20	0.38	1.00	0.06	0.03	4.64	76.90	4.29	0.08	171
	39-F2	13.40	0.03	0.94	0.00	0.02	4.17	76.50	3.60	0.07	201
	37-4	12.30	0.53	1.60	0.00	0.00	3.72	76.60	3.93	0.14	286
Cone Sheets											
	CS	13.31	0.08	0.11	0.00	0.00	4.11	76.68	5.72	0.01	
	CS-4	13.56	0.11	0.95	0.00	0.00	4.30	75.02	6.05	0.02	
	CS-5	13.56	0.16	0.83	0.00	0.00	4.33	75.46	5.60	0.06	
Country Rock											
	Laguna Arm.	18.92	0.27	6.97	2.01	0.04	2.91	66.71	1.66	0.51	
	GT-XTRY	13.34	0.40	0.69	0.00	0.04	4.20	76.56	4.71	0.07	

Table 1 (cont.)

Bulk Oxide and Rb concentrations for the Torres del Paine sample set.

		Al_2O_3	CaO	FeO	MgO	P_2O_5	K_2O	SiO_2	Na_2O	TiO_2	Rb
Feeder Zone											
	FZ-1	19.42	8.36	8.55	5.16	0.35	0.87	50.69	2.70	3.89	
	FZ-2	16.48	8.83	9.36	7.72	0.25	1.04	51.88	2.06	2.38	
Magmatic Features											
Felsic Veins	**GMT-5F**	14.56	1.38	0.75	0.00	0.00	3.74	76.51	3.00	0.06	
Felsic Veins	**TB-2**										
Felsic Veins	**TB-3**										
Comp. Dike Felsic	**CD-2**	15.20	0.31	2.39	0.00	0.03	4.18	72.19	5.38	0.32	
Comp. Dike Mafic	**CD-4**	17.66	6.92	8.73	4.44	0.08	1.08	55.48	4.19	1.42	
Basaltic Dike	**GT-9**	17.79	8.17	6.40	3.39	0.00	1.48	57.86	3.88	1.02	
Chilled Mafic Enclaves	**P10-16**	16.10	7.46	10.26	7.76	0.88	3.27	48.20	2.85	2.21	33
Chilled Mafic Enclaves	**P10-11**	15.80	7.52	9.29	7.47	0.36	3.59	49.50	3.79	2.08	78
Chilled Mafic Enclaves	**P11-8**	17.10	4.84	8.15	4.17	0.72	2.94	55.20	5.09	1.63	162

Table 1 (cont.)

Bulk Oxide and Rb concentrations for the Torres del Paine sample set.

		$^{87}Sr/^{86}Sr$	2SD	$^{208}Pb/^{204}Pb$	2SD	$^{207}Pb/^{204}Pb$	2SD	$^{206}Pb/^{204}Pb$	2SD
Granites									
	GMT-1	0.70540							
	GMT-2	0.70548	0.000009						
	GMT-3	0.70531	0.000001						
	SG-5	0.70669	0.000040						
	SG-3	0.70748	0.000040						
	SG-1	0.70706	0.000008						
	VG-3	0.70562	0.000006						
	VG-5	0.70644	0.000002						
	VG-8	0.70570	0.000031						
	C-44	0.70582	0.000027						
	Cig-1	0.70575							
	GT-0	0.70827							
	GT-1	0.70860							
	GT-15	0.71283							
	11_23			38.670		15.630		18.757	
	10_10	0.70501		38.714		15.633		18.785	
	CF_3	0.70569							
	037-5	0.70590							
	1340C	0.70591							
	13-15			38.689		15.631		18.779	
	039-A			38.681		15.630		18.773	
	13_10			38.692		15.634		18.770	
	CF-2	0.70534							
	10_20	0.70628							
	13_9			38.696		15.632		18.775	
	038_6	0.70622		38.678		15.631		18.768	
	038_2	0.70721							
Diorites									
	VF-16	0.70457							
	C-1			38.649	0.0045	15.631	0.0015	18.746	0.0015
	C-45	0.70442	0.000008						
	GMT-5M	0.70438	0.000007						
	P11-12	0.70442							
	P9-12	0.70436		38.666		15.629		18.758	
	P11-19	0.70422							

Table 2

Sr and Pb isotope data for the Torres del Paine sample set.

		$^{87}Sr/^{86}Sr$	2SD	$^{208}Pb/^{204}Pb$	2SD	$^{207}Pb/^{204}Pb$	2SD	$^{206}Pb/^{204}Pb$	2SD
	P11-7	0.70453							
	P13-3	0.70429							
	O13-12a			38.706		15.631		18.802	
	O13-12b			38.704		15.631		18.783	
	T1200	0.70456							
Gabbros									
	VF-11	0.70395							
	VF-14	0.70454							
	C-8			38.635	0.0014	15.625	0.0001	18.738	0.0008
	Cig-5	0.70423							
	P11-25	0.70410							
	P11-24	0.70411							
	O12-11	0.70390							
	P11-16	0.70436		38.632		15.631		18.716	
	P13-4	0.70527							
Aplites									
	10-19			38.671		15.644		18.886	
	9-16a			38.723		15.635		18.805	
	9-11MC			38.708		15.634		18.804	
Cone Sheets									
	CS-4			38.662	0.0072	15.627	0.0026	18.762	0.0031
Country Rock									
	Laguna Arm.	0.71480		38.677	0.0014	15.642	0.0002	18.772	0.0011
	GT-XTRY	0.71002		38.643	0.0048	15.636	0.0015	18.733	0.0002
Magmatic Features									
Felsic Veins	**GMT-5F**	0.70526	0.000014						
Comp. Dike Felsic	**CD-2**	0.70634	0.000041	38.660	0.0037	15.631	0.0016	18.761	0.0004
Comp. Dike Mafic	**CD-4**	0.70499	0.000027	38.640	0.0032	15.633	0.0016	18.734	0.0006
Chilled Mafic Enclaves	**P10-16**			38.670		15.634		18.767	
Chilled Mafic Enclaves	**P11-8**	0.70533							
Standards									
	SRM981			36.668	0.0069	15.486	0.0017	16.938	0.0011
	BCR			38.652	0.0065	15.616	0.0021	18.725	0.0016
	SRM987	0.71026	0.000019						
	Coral	0.70918	0.000035						
	E&A	0.70803	0.000011						

Table 2 (cont.)

Sr and Pb isotope data for the Torres del Paine sample set.

		$\delta^{56}Fe$	2SD	2SE	n
Granites					
	GMT-1	0.13	0.03	0.02	2
	GMT-2	0.16	0.01	0.01	2
	GMT-3	0.17	0.04	0.04	2
	VF-1	0.18	0.01	0.01	2
	SG-5	0.27	0.01	0.01	2
	SG-3	0.17	0.04	0.03	2
	SG-1	0.17	0.00	0.01	2
	VG-3	0.22	0.07	0.05	2
	VG-5	0.24	0.05	0.03	2
	VG-8	0.26	0.01	0.01	2
	C-44	0.21	0.09	0.04	4
	Cig-1	0.16	0.04	0.03	2
	GT-0	0.25	0.03	0.02	2
	GT-1	0.26	0.04	0.02	2
	GT-2	0.36	0.01	0.01	2
	GT-3	0.24	0.05	0.03	2
	GT-4	0.27	0.04	0.03	2
	GT-7	0.26	0.02	0.02	2
	GT-11	0.28	0.07	0.05	2
	GT-14	0.19	0.03	0.02	2
	GT-15	0.25	0.02	0.02	2
	ST-4	0.19	0.03	0.02	3
Diorites					
	GMT-4	0.12	0.01	0.01	2
	VF-2	0.11	0.01	0.01	2
	VF-3	0.11	0.04	0.03	2
	C-1	0.08	0.18	0.06	8
	C-45	0.16	0.12	0.06	4
	TB-1	0.15	0.04	0.03	2
	TB-5	0.05	0.15	0.09	3
	C-3	0.17	0.05	0.04	2
	GMT-5M	0.05	0.03	0.02	2

Table 3

Fe isotope data for the Torres del Paine sample set.

		δ^{56}Fe	2SD	2SE	n
Gabbros					
	VF-9	0.13	0.03	0.01	2
	VF-11	0.14	0.02	0.01	2
	VF-14	0.08	0.00	0.01	2
	C-8	0.13	0.01	0.01	2
	C-15	0.05	0.00	0.01	2
	C-22	0.16	0.08	0.04	5
	C-39	0.15	0.04	0.03	2
	Cig-5	0.07	0.01	0.01	2
	ST-5	0.13	0.07	0.04	3
Aplites					
	10-19	0.52	0.03	0.02	2
	31-6	0.36	0.02	0.01	2
	9-16a	0.28	0.04	0.03	2
	9-11MC	0.27	0.02	0.01	2
	39-F2	0.42	0.03	0.02	2
	37-4	0.35	0.04	0.03	3
Cone Sheets					
	CS	0.17	0.02	0.01	2
	CS-4	0.27	0.01	0.01	2
	CS-5	0.30	0.02	0.01	2
Country Rock					
	Laguna Arm.	0.05	0.03	0.02	2
	GT-XTRY	0.03	0.03	0.02	2
Feeder Zone					
	FZ-1	0.11	0.03	0.02	2
	FZ-2	0.10	0.03	0.02	3
Magmatic Features					
Felsic Veins	**GMT-5F**	0.19	0.19	0.05	2
Felsic Veins	**TB-2**	0.23	0.02	0.02	2
Felsic Veins	**TB-3**	0.30	0.12	0.07	3
Comp. Dike Felsic	**CD-2**	0.17	0.07	0.05	2
Comp. Dike Mafic	**CD-4**	0.12	0.05	0.03	2
Basaltic Dike	**GT-9**	0.18	0.00	0.01	2
Standards					
	UiFe	0.68	0.07	0.01	30
	BCR-2	0.07	0.09	0.02	25
	AGV-2	0.07	0.09	0.04	4
	RGM-2	0.22	0.06	0.03	4
	NOD-P	-0.53	0.07	0.04	4

Table 3 (cont.)

Fe isotope data for the Torres del Paine sample set.

References

Annen C., Scaillet B. and Sparks R. S. J. (2006) Thermal constraints on the emplacement rate of a large intrusive complex; the Manaslu Leucogranite, Nepal Himalaya. *J. Petrol.* **47**, 71-95.

Beard, B.L., Johnson, C.M., 2004. Inter-mineral Fe isotope variations in mantle-derived rocks and implications for the Fe geochemical cycle. *Geochemistry Geophysics Geosystems* **68**, 4727-4743.

Bilenker, L.D., Simon, A., Lundstrom, C.C., Gajos, N. (2012) Iron isotope fractionation among magnetite, pyrrhotite, chalcopyrite, rhyolite melt and aqueous fluid at magmatic hydrothermal conditions, *Trans AGU. Fall Meeting.*

Bindeman I.N., Lundstrom C. C., Bopp C. and Huang F. (2013) Stable isotope fractionation by thermal diffusion through partially molten wet and dry silicate rocks *Earth andPlanetaryScienceLetters* **365** 51–62

Boudreau A. E. (2003) IRIDIUM—a program to model reaction of silicate liquid infiltrating a porous solid assemblage. *Comput. Geosci.* **29**, 423–429.

Buddington, A.F., (1959), Granite emplacement with special reference to North America: *Geological Society of America Bulletin*, v. **70**, p. 671–747.

Coleman D. S., Gray W. and Glazner A. F. (2004) Rethinking the emplacement and evolution of zoned plutons; geochronologic evidence for incremental assembly of the Tuolumne Intrusive Suite, California. *Geology* **32**, 433-436.

Dominguez G., Wilkins G. and Thiemens M.H. (2011) The Soret effect and isotopic fractionation in high temperature silicate melts. *Nature* **473**, 70-73.

Gladu, A H. and Kamber, B.B., (2008) Pb purification by HBr-HCl and HBr-HNO_3 chemistry; a comparison. *Geochimica et Cosmochimica Acta*, **72**(12), A312-A312.

Glazner A. F., Bartley J. M., Coleman D. S., Gray W., and Taylor R. Z. (2004) Are plutons assembled over millions of years by amalgamtion from samll magma chambers? *GSA Today* **14**, 4-7.

Harrison T. M., Grove M., McKeegan K., Coath C. D., Lovera O.M. and Le Fort P. (1999) Origin and episodic emplacement of the Manaslu Intrusive Complex, Central Himalaya. *J. Petrol.* **40**, 3–19.

Heimann A., Beard B.L., Johnson C.M., 2008. The role of volatile exsolutions and subsolidus fluid/rock interactions in producing high 56Fe/54Fe ratios in siliceous igneous rocks. *Geochim. Cosmochim. Acta* **72**, 4379–4396.

Huang F., Lundstrom C.C., Ianno A. J., Boudreau A. E., Li J., Ferré E. C., Marshak S. and DeFrates J. (2009) Thermal Migration in Wet Andesite: Experiments and models suggesting a new mechanism of magma differentiation. *Geochimica et Cosmochimica Acta* **73**, 729-749.

Huang, F., Chakraborty, P., Lundstrom, C.C., Holmden, C., Glessner, J.J.G., Kieffer, S.W., Lesher, C.E., 2010. Isotope fractionation in silicate melts by thermal diffusion. *Nature* **464**, 396-399.

Kilian R. and Berhmann J.H. (2003) Geochemical constraints on the sources of Southern Chile Trench sediments and their recycling in arc magmas of the Southern Andes. *Journal of the Geological Society of London* **160**, 57–70.

Kyser T.K., Lesher C.E. and Walker D. (1998) The effects of liquid immiscibility and thermal diffusion on oxygen isotopes in silicate liquids. *Contributions to Mineralogy and Petrology* **133**, 373-381.

Lacks, D.J., Goel, G., Bopp, C.J., VanOrman, J.A., Lesher, C.E., Lundstrom, C., 2012. Isotope fractionation by thermal diffusion in silicate melts. Phys. Rev. Lett. 108, http://dx.doi.org/10.1103/PhysRevLett.108.065901, Article Number: 065901.

Lesher C.E. and Walker D. (1988) Cumulate Maturation and Melt Migration in a Temperature gradient. *Journal of Geophysical Research* **93**, 10295-10311.

Lesher C. E. and Walker D. (1991) Thermal diffusion in petrology. In Diffusion, Atomic Ordering, and Mass Transport. *Advances in Physical Geochemistry*, vol. **8** (ed. J. Ganguly). Springer-Verlag, New York, pp. 396–451.

Leuthold, J., Müntener, O., Baumgartner, L., Putlitz B., Ovtcharova M. and Schaltegger U. (2012) Time resolved construction of a bimodal laccolith (Torres del Paine, Patagonia). *Earth and Planetary Science Letters*, **325**, 85-92.

Lundstrom C.C. (2009) Hypothesis for origin of convergent margin granitoids and Earth's continental crust by thermal migration zone refining. *Geochim. Cosmochim Acta* **73**, 5709–5729.

Michel J., Baumgartner L., Putlitz B., Schaltegger U. and Ovtcharova M. (2008) Incremental growth of the Patagonian Torres del Paine laccolith over 90 kyrs. *Geology* **36**, 459-462.

Michael P.J. (1984) Chemical differentiation of the Cordillera Paine granite (southern Chile) by in situ fractional crystallization. *Contrib. Mineral. Petrol.* **87**, 179-195.

Michael P.J. (1991) Intrusion of basaltic magma into a crystallizing granitic magma chamber: The Cordillera del Paine pluton in southern Chile. *Contrib. Mineral. Petrol.* **108**, 396-418.

Petford, N., Cruden, A.R., McCaffrey, K.J.W., and Vigneresse, J.-L., (2000), Granite magma formation, transport and emplacement in the Earth's crust: *Nature*, v. **408**, p. 669–673.

Pitcher, W.S., and Berger, A.R., (1972), The geology of Donegal: a study of granite emplacement and unroofing, *Regional geology series: New York, Wiley-Interscience*, 435 p.

Poitrasson F. (2006) On the iron isotope homogeneity level of the continental crust. *Chemical Geology* **235**, 195-200.

Poitrasson, F., Freydier, R., 2005. Heavy iron isotope composition of granites determined by high resolution MC-ICP-MS. *Chem. Geol.* **222**, 123-147.

Poitrasson, F. Halliday, A. N., Lee, D-C., Levasseur, S., Teutsch, N. (2004) Iron isotope differences between earth, moon, mars and vesta as possible records of contrasted accretion mechanisms. *Earth and Planetary Science Letters*, **223**(3), 253-266.

Polyakov, V.B., Mineev, S.D., (2000) The use of Mössbauer spectroscopy in stable isotope geochemistry. *Geochim Cosmochim Acta* 64(5), 849-865.

Richter F.M., Watson E.B., Mendybaev R., Dauphas N., Georg B., Watkins J. and Valley J. (2009) Isotopic Fractionation of the Major Elements of Molten Basalt by Chemical and Thermal Diffusion. *Geochimica et Cosmochimica Acta* **73**, 4250-4263.

Richter F.M., Watson E. B., Mendybaev R., Teng F.-Z. and Janney P. (2008) Magnesium Isotope Fractionation in Silicate Melts by Chemical and Thermal Diffusion. *Geochimica et Cosmochimica Acta* **72**, 206-220.

Rudnick R. L. and Gao S. (2003) Composition of the continental crust. In The Crust, vol. **3** (ed. R. L. Rudnick) (eds. H. D. Holland and K. K. Turekian). Elsevier, Pergamon, Oxford, pp. 1–64.

Schauble E.A. (2004) Applying stable isotope fractionation theory to new systems. *Rev. Mineral. Geochem.* **55**, 65-111.

Schoenberg, R., von Blanckenburg, F., (2006) Modes of planetary-scale Fe isotope fractionation. *Earth Planet. Sci. lett.* **252**, 342-359.

Schuessler, J.A., Schoenberg, R., Sigmarsson, O., (2009) Iron and lithium isotope systematics of the Hekla volcano, Iceland - Evidence for Fe isotope fractionation during magma differentiation. *Chem. Geol.* **258**, 78-91.

Shahar, A., Young, E.D., Manning, C.E., (2008) Equilibrium high-temperature Fe isotope fractionation between fayalite and magnetite: an experimental calibration. *Earth Planet Sci Lett* **268**, 330-338.

Staubwasser, M., von Blanckenburg, F., Schoenberg R., (2006) Iron isotopes in the early marine diagenetic iron cycle, *Geology* **34** (8) 629–632.

Tappa M.J., Coleman D.S., Mills R.D. and Samperton K.M. (2011) The plutonic record of a silicic ignimbrite from the Latir volcanic field, New Mexico. *Geochem. Geophys. Geosyst.* **12**, Q10011, 16.

Taylor S. R. and White J. R. A. (1965) Geochemistry of andesites and the growth of continents. *Nature* **208**, 271–273.

Telus, M., Dauphas, N., Moynier, F., Tissot, F.L.H., Teng, F.Z., Nabelek, P.I., Craddock, P.R., Groat, L.A., (2012) Iron, zinc, magnesium and uranium isotopic fractionation during continental crust differentiation: The tale from migmatites, granitoids, and pegmatites. *Geochim. Cosmochim. Acta* **97**, 247-265.

Tuttle O. F. and Bowen N. L. (1958) Origin of granite in the light of experimental studies in the system NaAlSi3O8–KAlSi3O8– SiO2–H2O. Memoir—*Geological Society of America*, **74**, 153 pp.

Walker D., Jurewicz S. and Watson E. B. (1988) Adcumulus dunite growth in a laboratory thermal gradient. *Contributions to Mineralogy and Petrology* **99**, 306-319.

Appendix A

	Sample Name	Sample Type	Description	GPS * Denotes Approximate	Elevevation	Location Notes
North Wall Mafic Traverse						
	VF-1	**Granite**	**Typical Granite**	*50°57'23.0"S 73°03'30.0"W	*1180	
	VF-2	**Diorite**	**Homogenous Diorite**	"	"	
	VF-3	**Diorite**	**Homogenous Diorite**	"	"	
	VF-4	**Diorite**	**Mix Zone Diorite**	"	:	
	VF-6	**Diorite**	**Elongate Hornblendes**	50°57'31.2"S 73°03'36.4"W	*1046	
	VF-7	**Diorite**	**Homogenous Diorite**	50°57'31.7"S 73°03'37.6"W	*1044	
	VF-8	**Diorite**	**Mix Zone Diorite**	50°57'32.1"S 73°03'38.2"W	*1042	
	VF-9	**Gabbro**	**Homogenous Diorite**	50°57'32.5"S 73°03'39.1"W	*1042	
	VF-10	**Gabbro**	**Mix Zone Diorite**	50°57'36.3"S 73°03'56.2"W	944	
	VF-11	**Gabbro**	**Homogenous Diorite**	50°57'33.0"S 73°03'54.1"W	1007	
	VF-12	**Gabbro**	**Homogenous Diorite**	50°57'35.7"S 73°03'57.4"W	1011	
	VF-13	**Gabbro**	**Gabbro Felsite Wall Contact**	50°57'35.9"S 73°03'57.9"W	1011	
	VF-14	**Gabbro**	**Homogenous Gabbro Weathers Easily**	50°57'34.8"S 73°03'58.2"W	1029	
	VF-15	**Gabbro**	**Homogenous Gabbro**	50°57'34.1"S 73°03'58.4"W	*1020	
	VF-16	**Diorite**	**Homogenous Diorite**	50°57'33.5"S 73°03'58.6"W	*1020	
	VF-17	**Diorite**	**Diorite With Large Hornblende Crystals**	50°57'31.5"S 73°04'08.3"W	1023	
Northern Granite Mafic Traverse						
	GMT-1	**Granite**	**Typical Granite**	50°57'24.0"S 73°04'00.0"W	*1120	
	GMT-2	**Granite**	**Typical Granite**	50°57'25.4"S 73°04'01.9"W	1100	
	GMT-3	**Granite**	**Typical Granite Next To GMT-4 Diorite**	50°57'26.0"S 73°04'03.5"W	1088	
	GMT-4	**Diorite**	**Diorite Pod In Granite**	50°57'26.5"S 73°04'04.3"W	1080	
	GMT-5	**Gabbro**	**Gabbro With Cross Cutting Felsic Vein**	50°57'26.6"S 73°04'04.9"W	1060	
Tiburon Mafic Traverse						
	TB-1	**Diorite**	**Homogenous Diorite**	*50°58'04.8"S 73°04'31.8"W	*1060	
	TB-2	**Granite**	**Top Of Felsite (3m thick)**	"		
	TB-3	**Granite**	**Bottom of the Felsite (3m thick)**	"		
	TB-4	**Granite/Diorite**	**Bottom of Vein Plus Underlying Diorite**	"		
	TB-4 Dike	**Basalt**	**Basaltic Dike**	"		
	TB-5	**Dlorite**	**Homogenous Diorite**	"		
	TB-6	**Dlorite**	**Homogenous Diorite**	50°58'05.2"S 73°04'31.7"W	1045	
	TB-7	**Dlorite**	**Mix Zone Diorite**	"	"	10m above T2-1
	TB-8	**Dlorite**	**Homogenous Diorite**	"	"	8m above T2-1
	TB-9	**Dlorite**	**Homogenous Diorite**	50°58'11.1"S 73°04'32.5"W	*1020	
Tiburon Mafic Felsic Tongue Traverse						
	ST-1	**Diorite/Granite**	**Contact Sample Felsite and Underlying Diorite**	50°57'56.7"S 73°04'39.1"W	1113	
	ST-2	**Diorite**	**Homogenous Diorite**	50°57'59.0"S 73°04'37.6"W	1109	
	ST-3	**Diorite**	**Homogenous Diorite**	50°57'57.7"S 73°04'38.4"W	1106	
	ST-4	**Granite**	**Feslsite**	50°57'56.7"S 73°04'39.1"W	1113	
	ST-5	**Gabbro**	**Homogenous Gabbro Directly Below Felsite**	50°57'55.8"S 73°04'40.5"W	1119	
	ST-6	**Granite**	**Homogenous Granite**	50°57'54.5"S 73°04'40.9"W	1099	
	ST-7	**Diorite**	**Diorite with Felsic Veins**	50°57'54.5"S 73°04'40.6"W	1116	

Appendix A

List of samples arranged primarily by sample location. List includes brief sample description, GPS location and elevation information.

Sample Name	Sample Type	Description	GPS * Denotes Approximate	Elevevation	Location Notes
Castillo Mega Transect					
C-1	**Layered Diorite**	**Homogenous Diorite**	50°58'37.0"S 73°06'06.4"W	1260	4 meters above contact
C-2	**Layered Diorite**	**Homogenous Diorite**	"	"	3m above contact
C-3	**Layered Diorite**	**Homogenous Diorite**	"	"	1.5m above contact
C-4	**Layered Diorite**	**Homogenous Diorite**	"	"	.5m above contact
C-5	**Layered Diorite Upper Hornblende Gabbro**	**Contact Between The Two Units**	50°58'38.0"S 73°06'05.3"W	1257	contact
C-6	**Upper Hornblnde Gabbro**	**Homogenous Gabbro**	"	"	5 cm below contact
C-7	**Upper Hornblnde Gabbro**	**Homogenous Gabbro**	"	"	.3m below contact
C-8	**Upper Hornblnde Gabbro**	**Homogenous Gabbro**	"	"	1.5m below contact
C-9	**Upper Hornblnde Gabbro**	**Homogenous Gabbro**	"	"	5m above C-10
C-10	**Upper Hornblnde Gabbro**	**Homogenous Gabbro**	50°58'38.9"S 73°06'02.3"W	1247	
C-11	**Upper Hornblnde Gabbro**	**Homogenous Gabbro**	"	"	
C-12	**Upper Hornblnde Gabbro**	**Homogenous Gabbro**	50°58'39.5"S 73°06'00.5"W	1250	
C-13	**Upper Hornblnde Gabbro**	**Homogenous Gabbro**	"	"	Between C-11 and C-13
C-14	**Upper Hornblnde Gabbro**	**Homogenous Gabbro**	50°58'39.3"S 73°05'59.2"W	1239	
C-15	**Upper Hornblnde Gabbro**	**Homogenous Gabbro**	50°58'38.8"S 73°05'59.2"W	1213	
C-16	**Upper Hornblnde Gabbro**	**Homogenous Gabbro**	"	"	3m below C15
C-17	**Diorite**	**Homogenous Diorite**	50°58'38.8"S 73°05'58.5"W	1196	
C-18	**Gabbro**	**Homogenous Gabbro**	"	"	Next to C17
C-19	**Gabbro**	**Homogenous Gabbro**	"	"	5m below C18
C-20	**Diorite/Gabbro**	**Mix Zone Diorite/Gabbro**	50°58'36.3"S 73°05'57.8"W	1190	
C-21	**Gabbro**	**Homogenous Gabbro**	"	"	
C-22	**Diorite/Gabbro**	**Mix Zone Diorite/Gabbro Finer Grained**	"	"	
C-23	**Diorite/Gabbro**	**Mix Zone Diorite/Gabbro**	"	"	
C-24	**Diorite**	**Homogenous Diorite**	50°58'38.6"S 73°05'55.0"W	1153	
C-25	**Diorite**	**Outcrop Has Rusty Appearance**	"	"	3m below C24
C-27	**Diorite**	**Diorite With Large Hornblende Crystals**	50°58'39.3"S 73°05'53.4"W	1128	
C-28	**Diorite**	**Mix Zone Diorite**	"	"	
C-29	**Diorite**	**Homogenous Diorite**	50°58'40.5"S 73°05'52.4"W	1107	Going laterally
C-30	**Diorite**	**Mix Zone Veining Diorite**	"	"	
C-31	**Diorite**	**Mix Zone Veining Diorite**	50°58'42.2"S 73°05'55.1"W	1138	
C-32	**Lower Hornblende Gabbro**	**Homogenous Gabbro**	"	"	
C-33	**Lower Hornblende Gabbro**	**Mix Zone Gabbro**	50°58'40.5"S 73°05'51.8"W	1111	
C-34	**Lower Hornblende Gabbro**	**Homogenous Gabbro**	"	"	1m below C33
C-35	**Lower Hornblende Gabbro**	**Homogenous Gabbro**	"	"	1m below C34
C-36	**Lower Hornblende Gabbro**	**Homogenous Gabbro**	"	"	Contact-0.3cm below 35
C-37	**Lower Hornblende Gabbro**	**Mix Zone Gabbro**	"	"	Directly next to 36
C-38	**Lower Hornblende Gabbro**	**Homogenous Gabbro**	"	"	1m below C37
C-39	**Lower Hornblende Gabbro**	**Homogenous Gabbro**	"	"	1m below C38
C-40	**Lower Hornblende Gabbro**	**Mix Zone Gabbro**	"	"	1m below 39
C-41	**Lower Hornblende Gabbro**	**Homogenous Gabbro**	50°58'41.0"S 73°05'50.1"W	1102	3m above felsic pod
C-42	**Lower Hornblende Gabbro**	**Mix Zone Gabbro**	"	"	1m above felsic pod
C-43	**Gabboro/Granite**	**Contact**	"	"	Contact
C-44	**Granite**	**Granite Pod**	50°58'41.1"S 73°05'50.3"W	1085	1m below contact
C-45	**Diorite**	**Homogenous Diorite**	50°58'46.7"S 73°05'54.6"W	1072	
C-47	**Diorite**	**Diorite With Felsic Veins**	"	"	
C-48	**Diorite**	**Mix Zone Diorite**	"	"	
C-49	**Diorite**	**Homogenous Diorite**	"	"	
C-50	**Diorite**	**Homogenous Diorite**	50°58'47.3"S 73°05'55.7"W	1063	

Appendix A (cont.)

List of samples arranged primarily by sample location. List includes brief sample description, GPS location and elevation information.

Sample Name	Sample Type	Description	GPS	Elevevation	Location Notes
			* Denotes Approximate		
Castillo Felsic Pod Transect					
Cig-1	Granite	Homogenous Granite	50°58'39.3"S 73°05'48.2"W	1093	
Cig-2	Granite	Homogenous Granite	"		
Cig-3	Granite	Homogenous Granite	"		
Cig-4	Granite/Gabbro	Contact Sample	"		
Cig-5	Gabbro	Mix Zone Gabbro	50°58'39.3"S 73°05'48.5"W	1079	
Cuernos Cone Sheet					
CS-1	Country Rock	Mudstone	51°00'52.2"S 72°58'32.5"W	170	
CS-2	Country Rock	Mudstone	"	"	
CS-3	Country Rock/ Cone Sheet	Contact	"	"	
CS-4	Cone Sheet	Prophyritc Granite, Spherical Quartz (Middle)	"	"	
CS-5	Cone Sheet	Prophyritc Granite, Spherical Quartz Top)	"	"	
CS-6	Country Rock	Mudstone	"	"	
Torres Valley Cone Sheet					
CS p1/p2	Cone Sheet	Prophyritc Granite, Weathered In Forest	50°56'44.0"S 72°56'24.1"W	803	
CS-MD	Cone Sheet	Prophyritc Granite, Weathered In Forest	?		
Valle Silencio Composite Dike					
CD-0	Country Rock/Basalt	Metamudstone/Upper Basaltic Contact	50°56'07.2"S 72°59'40.9"W	1130	
CD-1	Basalt/Granite	Upper Basaltic/Felsite Contact	50°56'07.2"S 72°59'40.5"W	"	
CD-2	Granite	Top Of Felsic Component	50°56'06.6"S 72°59'40.5"W	"	
CD-3	Granite	Bottom of Felsic Component	50°56'06.3"S 72°59'40.8"W	"	
CD-4	Basalt	Lower Basaltic Component	50°56'06.5"S 72°59'40.5"W	"	
Valle Silencio Mafic Enlcaves					
ME-1	Mafic Enclave	Mafic Enclave	50°56'56.0"S 73°00'14.2"W	1312	
ME-2	Mafic Enclave	Mafic Enclave	50°56'55.9"S 73°00'14.3"W	1310	
ME-3	Mafic Enclave	Mafic Enclave	50°56'55.4"S 73°00'13.8"W	1309	
Valle Silencio Miscellaneous					
VS-1	Basalt	Dike	50°55'30.9"S 72°58'17.6"W	837	
VS-2	Aplite	Float with 2mm Pyrite Crystal	50°55'49.7"S 72°59'25.1"W	1045	
VS-3	Aplite	Below Country Rock/ Granite Contact	50°56'05.5"S 72°59'40.7"W	1114	
VS-4	Basalt	Dike In Country Rock	?		
Sediment Granite Transect					
VG-1	Country Rock	Mudstone	50°56'09.4"S 72°59'41.3"W	1168	
VG-2	Granite	Homogenous Granite	50°56'09.8"S 72°59'41.4"W	1170	
VG-3	Granite	Homogenous Granite	50°56'11.5"S 72°59'45.5"W	1159	
VG-4	Granite	Homogenous Granite	50°56'14.0"S 72°59'47.3"W	*1200	
VG-5	Granite	Homogenous Granite	50°56'20.8"S 72°59'54.6"W	1223	
VG-6	Granite	Homogenous Granite	*50°56'34.0"S 73°00'11.0"W	*1200	
VG-7	Granite	Homogenous Granite	*50°56'40.0"S 73°00'15.0"W	*1201	
VG-8	Granite	Homogenous Granite	50°56'53.5"S 73°00'13.2"W	1310	
SG-1	Brecciated Granite	Low Mafic Content Granite	50°56'05.2"S 72°59'38.9"W	1121	
SG-2	Brecciated Granite	Low Mafic Content Granite	50°56'04.9"S 72°59'36.8"W	1133	
SG-3	Country Rock/Brecciated Granite	Contact	50°56'04.6"S 72°59'36.6"W	1138	
SG-4	Country Rock/Brecciated Granite	Contact	50°56'03.8"S 72°59'35.9"W	1114	
SG-5	Brecciated Granite	Low Mafic Content Granite	50°56'02.5"S 72°59'34.7"W	1125	
SG-6	Country Rock/Brecciated Granite	Stringers Of Digested Country Rock In Granite	50°56'02.3"S 72°59'33.3"W	1130	
C-49	Diorite	Homogenous Diorite	"	"	
C-50	Diorite	Homogenous Diorite	50°58'47.3"S 73°05'55.7"W	1063	

Appendix A (cont.)

List of samples arranged primarily by sample location. List includes brief sample description, GPS location and elevation information.

	Sample Name	Sample Type	Description	GPS	Elevevation	Location Notes
				* Denotes Approximate		
Feeder Zone						
	FZ-Sed	**Country Rock**	**Mudstone**	50°58'06.3"S 73°11'22.8"W	500	
	FZ-1	**Gabbro**	**Homogenous Gabbro**	"	"	
	FZ-2	**Gabbro**	**Layered Gabbro**	"	"	
	FZ-3	**Gabbro**	**Layered Gabbro**	50°58'05.6"S 73°11'20.3"W	538	
	FZ-4	**Gabbro**	**Gabbro Pods With Felsic Rinds**	50°58'04.3"S 73°11'19.5"W	?	
	FZ-5	**Gabbro**	**Euhedral Crystals in Vapor Pocket**	50°58'03.4"S 73°11'10.7"W*	?	
	FZ-6	**Diorite**	**Mix Zone Diorite**	"	"	
	FZ-7	**Diorite**	**Homogenous Diorite**	50°58'03.5"S 73°11'14.6"W	614	
	FZ-8	**Diorite**	**Mix Zone Diorite**	"	"	
	FZ-9	**Felsic Dike**	**Felsic Dike**	"	"	
	FZ-10	**Felsic Dike**	**Felsic Dike**	"	"	
	FZ-11	**Diorite**	**Mix Zone Diorite**	50°58'05.5"S 73°11'11.8"W	587	
Mirador Granite Transect						
	GT-Xtry	**Country Rock**	**Homogenous Granite**	50°57'23.4"S 72°56'59.8"W	1406	
	GT-0	**Granite**	**Homogenous Granite**	"	"	
	GT-1	**Granite**	**Homogenous Granite**	50°57'23.4"S 72°56'59.8"W	1406	
	GT-2	**Granite**	**Homogenous Granite**	50°57'24.0"S 72°57'03.1"W	1413	
	GT-3	**Granite**	**Homogenous Granite**	"	"	in between 1 & 4
	GT-4	**Granite**	**Homogenous Granite**	"	"	in between 1 & 4
	GT-5	**Granite**	**Homogenous Granite**	50°57'23.4"S 72°57'02.0"W	1388	
	GT-6	**Granite**	**Homogenous Granite**	"	"	in between 4 & 7
	GT-7	**Granite**	**Homogenous Granite**	"	"	in between 4 & 8
	GT-8	**Granite**	**Homogenous Granite**	50°57'23.4"S 72°57'03.1"W	1372	
	GT-9	**Granite**	**Homogenous Granite**	"	"	next to 9
	GT-10	**Granite**	**Homogenous Granite**	50°57'20.4"S 72°57'07.5"W	1323	
	GT-11	**Granite**	**Homogenous Granite**	float		
	GT-12	**Granite**	**Homogenous Granite**	50°57'19.5"S 72°57'07.5"W	1345	
	GT-13	**Granite**	**Homogenous Granite**	50°57'20.4"S 72°57'14.6"W	1337	
	GT-14	**Granite**	**Homogenous Granite**	50°57'23.2"S 72°57'22.8"W	1378	
	GT-15	**Granite**	**Homogenous Granite**	*50°57'08.0"S 72°57'45.0"W	*1100	

Appendix A (cont.)

List of samples arranged primarily by sample location. List includes brief sample description, GPS location and elevation information.